Seasonal differences in formation processes of oxidized organic aerosol near Houston, TX

Qili Dai[1, 2], Benjamin C. Schulze[2, 3], Xiaohui Bi[1, 2], Alexander A.T. Bui[2], Fangzhou Guo[2], Henry W. Wallace[2, 4], Nancy P. Sanchez[2], James H. Flynn[5], Barry L. Lefer[5, 6], Yinchang Feng[1*], Robert J. Griffin[2, 7]

[1] State Environmental Protection Key Laboratory of Urban Ambient Air Particulate Matter Pollution Prevention and Control, College of Environmental Science and Engineering, Nankai University, Tianjin 300350, China

[2] Department of Civil and Environmental Engineering, Rice University, Houston, TX, 77005

[3] Now at Department of Environmental Science and Engineering, California Institute of Technology, Pasadena, CA, 91125

[4] Now at Washington State Department of Ecology, Lacey WA, 98503

[5] Department of Earth and Atmospheric Sciences, University of Houston, Houston, TX, 77004

[6] Now at Division of Tropospheric Composition, NASA, Washington, DC, 20024

[7] Department of Chemical and Biomolecular Engineering, Rice University, Houston, TX, 77005

[*]Corresponding author: Yinchang Feng (fengyc@nankai.edu.cn)

Abstract

Submicron aerosol was measured to the southwest of Houston, Texas during winter and summer 2014 to investigate its seasonal variability. Data from a high-resolution time-of-flight aerosol mass spectrometer (HR-ToF-AMS) indicated that organic aerosol (OA) was the largest component of non-refractory submicron particulate matter (NR-PM_1) (on average, 38 ± 13% and 47 ± 18% of the NR-PM_1 mass loading in winter and summer, respectively). Positive matrix factorization (PMF) analysis of the OA mass spectra demonstrated that two classes of oxygenated OA (less and more-oxidized OOA, LO and MO) together dominated OA mass in summer (77%) and accounted for 39% of OA mass in winter. The fraction of LO-OOA (out of total OOA) is higher in summer (70%) than in winter (44%). Secondary aerosols (sulfate+nitrate+ammonium+OOA) accounted for ~76% and 88% of NR-PM_1 mass in winter and summer, respectively, indicating NR-PM_1 mass was driven mostly by secondary aerosol formation regardless of the season. The mass loadings and diurnal patterns of these secondary aerosols show a clear winter/summer contrast. Organic nitrate (ON) concentrations were estimated using the NO_x^+ ratio method, with contributions of 31-66% and 9-17% to OA during winter and summer, respectively. The estimated ON in summer strongly correlated with LO-OOA (r= 0.73) and was enhanced at nighttime.

The relative importance of aqueous-phase chemistry and photochemistry in processing OOA was investigated by examining the relationship of aerosol liquid water content (LWC) and the sum of ozone (O_3) and nitrogen dioxide (NO_2) (O_x=O_3+NO_2) with LO-OOA and MO-OOA. The processing mechanism of LO-OOA apparently depended on relative humidity (RH). In periods of RH <80%, aqueous-phase chemistry likely played an important role in the

formation of wintertime LO-OOA, whereas photochemistry promoted the formation of summertime LO-OOA. For periods of high RH >80%, these effects were opposite those of low RH periods. Both photochemistry and aqueous-phase processing appear to facilitate MO-OOA formation except during periods of high LWC, which is likely a result of wet removal during periods of light rain.

The nighttime increases of MO-OOA during winter and summer were 0.013 and 0.01 μg MO-OOA per μg of LWC, respectively. The increase of LO-OOA was larger than that for MO-OOA, with increase rates of 0.033 and 0.055 μg LO-OOA per μg of LWC at night during winter and summer, respectively. On average, the mass concentration of LO-OOA in summer was elevated by nearly 1.2 μg m^{-3} for a ~20 μg change in LWC, which was accompanied by a 40 ppb change in O_x.

1 Introduction

Tropospheric particulate matter (PM) has adverse effects on air quality, visibility, and ecosystems and participates in climate forcing (Watson, 2002; Grantz et al., 2003; Racherla and Adams, 2006; Tai et al., 2010; Liu et al., 2017). The various effects of PM depend on its physical, chemical and optical properties, which are determined by its emission, formation and evolution/aging processes. Atmospheric PM can either be directly emitted from primary sources (fossil fuel combustion, soil dust, sea salt, biomass burning, etc.) or formed through chemical reactions of gaseous precursors, as is the case for secondary inorganic sulfate (SO_4^{2-}) and nitrate (NO_3^-) and secondary organic aerosol (SOA). Understanding the source

contributions and formation pathways of PM is essential for mitigating its effects (Jimenez et al., 2009).

Houston, TX, is of great interest to the scientific community with respect to air quality, as it is the fourth most populous city in the United States (U.S.) and is well known for its energy and chemical industries. Numerous efforts, from modelling (McKeen et al., 2009; Li et al., 2015; Ying et al., 2015) to field measurements (for example, TexAQS 2000 and II (Bates et al., 2008; Parrish et al., 2009; Atkinson et al., 2010), Go-MACCS (McKeen et al., 2009; Parrish et al., 2009), TRAMP2006 (Mao et al., 2010; Cleveland et al., 2012), GC-ARCH (Allen and Fraser, 2006), SHARP (Olaguer et al., 2014), and DISCOVER-AQ (Bean et al., 2016; Leong et al., 2017)) have been made in the Houston metropolitan area during the past two decades, providing critical insights into our understanding of air quality and atmospheric chemistry with respect to the sources and formation of PM. Previous field campaigns underscore that OA accounts for a major fraction of non-refractory submicron PM (NR-PM_1) in Houston (Bates et al., 2008; Russell et al., 2009; Cleveland et al., 2012; Brown et al., 2013; Bean et al., 2016; Leong et al., 2017; Wallace et al., 2018). The spatial variation of NR-PM_1 in Houston was investigated by Leong et al. (2017), who divided greater Houston into two zones based on marked differences in NR-PM_1 levels, characteristics, and dynamics measured at 16 sampling locations. Zone 1 is northwest of Houston and is dominated by SOA likely driven by nighttime biogenic organic nitrate (ON) formation. Intensive attention has been paid recently to such anthropogenic-biogenic interactions (Bahreini et al., 2009; Bean et al., 2016). Zone 2 is the industrial/urban area south/east of Houston. Wallace et al. (2018) found mobile source exhaust

and petrochemical emissions likely are the most important factors impacting the NR-PM_1 and trace gases at a site in Zone 2.

Formation of SOA in clouds and the aqueous phase of aerosol particles has been reported worldwide (Lim et al., 2010; Ervens et al., 2011; Xu et al., 2017). Given that both photochemical oxidation and aqueous-phase chemistry are conducive to the formation of SOA, it is of interest to compare the relative importance of photochemistry and aqueous-phase chemistry for SOA formation in different seasons. The roles of photochemistry and aqueous-phase processing on SOA formation and evolution in different seasons in Beijing have been investigated by Hu et al. (2016) and Xu et al. (2017). Generally, aqueous-phase processing has a dominant influence on the formation of more oxidized SOA and photochemistry plays a major role in the formation of less oxidized SOA in summer and winter in Beijing, while the relative importance of these two pathways in the formation processes of SOA in autumn is different from those in summer and winter. The relative roles of aqueous-phase and photochemical processes in the formation of SOA likely vary with location and time. The seasonal differences in the spectral patterns, oxidation degrees and contributions of SOA may result from different volatile organic compound (VOC) precursors, meteorological conditions and atmospheric oxidizing capacity, which are not well understood in Houston, particularly in different seasons.

This study presents observations of NR-PM_1 from two high-resolution time-of-flight AMS (HR-ToF-AMS) measurement campaigns conducted during the winter and summer of 2014 at a site in the suburbs of Houston, where industrial and vehicular emission sources and photochemical processes are likely to play an important role in NR-PM_1 formation (Leong et

al., 2017). In addition to local emissions, this site was possibly impacted by regional marine aerosol transported from the Gulf of Mexico (Schulze et al., 2018). The aims of this work are to (1) investigate the seasonal characteristics of NR-PM_1 in the Houston area, (2) characterize the primary and secondary sources by applying positive matrix factorization (PMF) analysis to the measured OA mass spectra, and (3) evaluate the seasonal dependence of SOA composition and formation, with a main focus on the relative effects of photochemistry and aqueous-phase chemistry.

2 Materials and Methods

2.1 Sampling Site and Campaigns

Instrumentation was deployed in the University of Houston/Rice University Mobile Air Quality Laboratory (MAQL), as described in Leong et al. (2017) and Wallace et al. (2018). The winter campaign was conducted from February 3 through February 17, 2014, and the summer campaign was conducted from May 1 to May 31, 2014. The measurement site was located on the campus of University of Houston Sugar Land (UHSL) (29.5740 °N, 95.6518 °W). The campus is situated southwest of downtown and the Houston Ship Channel (HSC). The map of the measurement site is presented in Fig. S1 in the Supplemental Information (SI). The nearby interstate highway (I-69) extends to the west of downtown and serves as a major traffic emission source. The W.A. Parish Generating Station, a coal-fired power plant that is the largest electricity generating facility in Texas, is ~6 miles south of the site (Fig. S1). The data collected in the winter campaign are limited in duration; thus, the following discussion focuses

primarily on the summer campaign. The label of "winter/summer" in the text denotes the measurement period in the winter/summer.

2.2 Measurements

The data used in this paper are reported in local time, which is 6 and 5 hours behind Universal Coordinated Time in winter and summer, respectively. The details regarding the instrumental setup and data processing of these measurements were the same as described in Wallace et al. (2018). The NR-PM_1 composition was measured using an Aerodyne HR-ToF-AMS (DeCarlo et al., 2006; Canagaratna et al., 2007). A $PM_{2.5}$ Teflon®-coated cyclone inlet was installed above the MAQL at a height of 6 m above ground to remove coarse particles and to introduce air into the sampling line at a rate of 16.7 SLPM. A Nafion dryer (Perma Pure, LLC) was mounted upstream of the HR-ToF-AMS to dry the sample to below 45% relative humidity (RH). Particles are focused into a narrow beam via an aerodynamic lens and accelerated under high vacuum into the particle sizing measurement chamber. After passing the particle sizing chamber, the non-refractory components are flash vaporized at near 600^{o}C and ionized using electron impact at 70 eV. Ionized mass fragments are then transmitted directly into the time-of-flight region so that the mass spectra can be obtained. In this study, the HR-ToF-AMS was operated in "V-mode" to obtain the non-refractory chemical components with a higher sensitivity, lower mass spectral resolution compared to the "W-mode." Ionization efficiency (IE) calibration was performed monodisperse ammonium nitrate (NH_4NO_3) at the beginning and end of each campaign. Filtered ambient air was sampled every two days for approximately 20 to 30 min to provide a baseline of signal for the HR-ToF-AMS during

147 campaigns. The detection limits, (Table S1 in the SI) were calculated by multiplying the
148 standard deviations of the filter periods by three.

149 Trace gas mixing ratios and meteorological parameters also were measured on the MAQL
150 during the campaigns. Carbon monoxide (CO) was measured with high-resolution cavity
151 enhanced direct-absorption spectroscopy (Los Gatos Research, Inc.), and sulfur dioxide (SO_2)
152 was quantified using a pulsed fluorescence analyzer (ThermoFischer Scientific, model
153 43i-TLE). Nitric oxide (NO) and nitrogen dioxide (NO_2) were measured with a
154 chemiluminescence monitor with a UV-LED NO_2 photolytic converter on the NO_2 channel
155 (AQD, Inc.) The total reactive nitrogen (NO_y) was measured with a Thermo 49c-TL with a
156 heated Mo inlet converter. Ozone (O_3) mixing ratio was measured with ultraviolet absorption
157 (2BTech, Inc., model 205). Meteorological parameters including ambient temperature, solar
158 radiation, RH, wind speed (WS), and wind direction (WD) were measured using an RM Young
159 meteorological station. Precipitation totals from a nearby Texas Commission on Environmental
160 Quality (TCEQ) monitor site (EPA Site: 48_157_0696) were downloaded from TCEQ website.

161 **2.3 Data Processing**

162 The HR-ToF-AMS data analysis was performed using SQUIRREL v.1.56A and PIKA
163 v.1.19D in Igor Pro 6.37 (Wave Metrics Inc.). The relative IEs were applied to OA (1.4), SO_4^{2-}
164 (1.2), NO_3^- (1.1), NH_4^+ (4.0), and chloride (Cl^-, 1.3) following the standard data analysis
165 procedures. The composition-dependent collection efficiency was applied to the data based on
166 Middlebrook et al. (2012). Elemental ratios (H/C, O/C and N/C, where H is hydrogen, C is
167 carbon, N is nitrogen) and the ratio of organic mass to organic carbon (OM/OC) were generated

using the procedures described by Canagaratna et al. (2015). Example data are shown in Figure S2.

2.3.1 Quantification of the contributions of ON and Methanesulfonic Acid (MSA)

Estimation of ON. The mass loading of NO_3^- measured by HR-ToF-AMS includes both organic and inorganic NO_3^-. The fragmentation ratio of NO_2^+ to NO^+ (NO_x^+ ratio) is different for ON and inorganic NO_3^- (Farmer et al., 2010; Fry et al., 2013), and the NO_2^+ and NO^+ mass loadings for ON ($NO_{2,ON}$ and NO_{ON}) can be estimated using the method proposed by Farmer et al. (2010):

$$NO_{2,ON} = \frac{NO_{2,obs} \times (R_{obs} - R_{NO_3NH_4})}{R_{ON} - R_{NO_3NH_4}} \quad (1)$$

$$NO_{ON} = NO_{2,ON} / R_{ON} \quad (2)$$

where R_{obs} is the ambient NO_x^+ ratio (0.531, 0.260 for the winter and summer campaign, respectively; see Fig. S3 for details). $R_{NO_3NH_4}$(NO_x^+ ratio of NH_4NO_3) is determined by IE calibration using monodisperse NH_4NO_3 before and after the campaigns. The average of the two IE calibrations was used as the $R_{NO_3NH_4}$ for the campaign (0.588, 0.381 for the winter and summer campaigns, respectively), which is comparable with the value reported elsewhere (Xu et al., 2015; Zhu et al., 2016). The value of R_{ON} is hard to determine because it varies with instruments and precursor VOCs (Fry et al., 2013). Previous studies found that isoprene was the main biogenic VOC (BVOC) in Houston (Leuchner and Rappengluck, 2010; Kota et al., 2014), and Brown et al. (2013) reported that monoterpenes and isoprene were frequently present within the nocturnal boundary layer in the Houston area and underwent rapid oxidation, mainly by nitrate radical (denoted as $NO_3^{\cdot}$ with a dot to differentiate it from aerosol NO_3^-). Given the

abundance of monoterpene and isoprene in the Houston area, similar to Xu et al. (2015), we assume organic nitrates formed via isoprene and beta-pinene oxidation are representative. Fry et al. (2013) assumed that the $R_{ON}/R_{NH_4NO_3}$ value is instrument-independent, and further estimated the average $R_{ON}/R_{NH_4NO_3}$ of 2.25 for the organic nitrate standards. The $R_{ON}/R_{NH_4NO_3}$ values vary with precursor VOC. We utilized the $R_{ON}/R_{NH_4NO_3}$ of isoprene (2.08, (Bruns et al., 2010)) and beta-pinene organic nitrates (3.99, (Boyd et al., 2015)) from the literature to obtain an estimation range of R_{ON} by using the NO_x^+ method.

The measured NO_x^+ ratio can be used to separately quantify ammonium and organic nitrates as:

$$ON_{frac} = \frac{(R_{obs} - R_{NO3NH4})(1+R_{ON})}{(R_{ON} - R_{NO3NH4})(1+R_{obs})} \quad (3)$$

The nitrate functionality from organic nitrate was calculated as:

$$NO_{3,ON} = ON_{frac} \times NO_3^- \quad (4)$$

Thus, the nitrate functionality from inorganic nitrate (assuming NH_4NO_3 is the solely important inorganic nitrate in the submicron mode) can be calculated as:

$$NO_{3,AN} = \left(1 - ON_{frac}\right) \times NO_3^- \quad (5)$$

The accurate estimation of the total mass of ON via this method is uncertain as the actual molecular weight of the particle-phase species is unclear. The mass range of ON is estimated by assuming that the average molecular weights of organic molecules with nitrate functional groups are 200 to 300 g mol^{-1} (Surratt et al., 2008; Rollins et al., 2012). Previous work found that the $NO_3^{\cdot}$ reaction with monoterpenes resulted in significant SOA formation and that a hydroperoxy nitrate ($C_{10}H_{17}NO_5$) was likely a major $NO_3^{\cdot}$-oxidized terpene product in the southeastern U.S. (Ayres et al., 2015). Here, we use the molecular weight of $C_{10}H_{17}NO_5$ (231 g mol^{-1}) to calculate

the ON mass. Example periods of significant ON contribution to PM are given in Fig. S4. While the values of ON concentration estimated using this method are presented in the text, the result of estimated ON including uncertainties is available in Table S2.

Estimation of methane sulfonic acid (MSA). During the two campaigns, there is no significant organic sulfur contribution from ion fragments other than $CH_3SO_2^+$. The concentration of MSA was estimated as:

$$C_{MSA} = \frac{C_{CH3SO2}}{f_{MSA,\,CH3SO2}} \quad (6)$$

where C_{CH3SO2} is the concentration of ion fragment $CH_3SO_2^+$ (*m/z*=78.99) and the fraction of $CH_3SO_2^+$ to the total signal intensity of all the fragments of pure MSA, $f_{MSA,CH3SO2}$, is 5.55%. This values was observed for the mass spectra of pure MSA in laboratory experiments (Schulze et al., 2018) and is comparable to previous work (Huang et al., 2015).

2.3.2 PMF Analysis

The PMF technique has been used widely for source apportionment (Paatero and Tapper, 1994), including with HR-TOF-AMS data (Ulbrich et al., 2009; Zhang et al., 2011). The high-resolution NR-PM_1 OA mass spectra matrix (mass-to-charge ratio, m/z =12 to m/z=130) and the associated error matrix obtained by using PIKA v 1.19 D were used for PMF analysis. Data were prepared according to the protocol proposed by Ulbrich et al. (2009) and Zhang et al. (2011) prior to PMF analysis. The PMF model was used to decompose the measured OA mass spectra matrix by solving:

$$\mathrm{X} = \mathrm{GF} + E = \sum_{p=1}^{J} G_{ip} F_{pj} + E_{ij} \quad (7)$$

where X is the $m \times n$ matrix of measurement data, the *m* rows of X are the OA mass spectra measured at each time step, the *n* columns of X are the time series of each organic m/z, and *p* is the number of factors. G_{ip} is the matrix that denotes the contributions of factor *p* at time step *i*, and F_{pj} represents the factor mass spectral profiles. E is the residual matrix. The least-squares algorithm is used to fit the data to minimize iteratively a quality of fit parameter, Q:

$$Q = \sum_I \sum_J (E_{ij}/\sigma_{ij})^2 \quad (8)$$

where σ_{ij} is the matrix of estimated errors of the data.

Solutions using PMF with 2 to 7 factors were explored. The best solution with the optimum number of factors was evaluated carefully using an open source PMF evaluation tool (PET v 2.08D, (Ulbrich et al., 2009)) following the procedures described in Zhang et al. (2011). Selection criteria included 1.) variation of the ratio of Q to expected Q_{exp} ($mn-p(m+n)$, the degrees of freedom of the fitted data (Paatero et al., 2002)) after adding an additional factor, 2.) agreement between the reconstructed OA mass concentrations and the measured concentrations, 3.) scaled residuals for the different ion fragments included in the dataset and variations of the residual of the solution as a function of time, 4.) agreement between factor time series and time series of external tracers/individual ions, and 5.) examination of factor profiles. The last two are considered to determine the physical meaningfulness of the factors. The PMF solution with factor numbers greater than five and four for winter and summer dataset, respectively, yielded no new distinct and physical meaningful factors. The Q/Q_{exp} and the factors obtained for different FPEAK (from -1 to 1 with a step value of 0.2) values resulted in a small difference in the OA components. Because of the lowest Q/Q_{exp} and because the use of FPEAK values

different from 0 did not improve the correlations between PMF factors and potentially associated tracers, the five- and four-factors solutions with FPEAK=0 can be well interpreted in winter and summer, respectively. The convergence of the PMF model containing five- and four-factors were examined by running each model from fifteen different starting values (SEEDs 0-30 with a step value of 2). The small variation observed in Q/Q_{exp} and the mass fraction of different factors as SEED changed indicates the solutions were stable. As a result, SEED 0 was chosen for the final solution. The factors were interpreted as hydrocarbon-like OA (HOA), biomass burning OA (BBOA), cooking OA (COA, identified only in the winter campaign), and two oxidized OA (named less-oxygenated (LO-) OOA and more-oxygenated (MO-) OOA). The data treatment, factor selection and interpretation are detailed in the SI. As suggested by El-Sayed et al. (2016), drying of aerosol water may have led to the evaporation of condensed-phase organics. Thus, the resolved mass concentrations of OA factors here are a lower-bound, conservative estimate due to losses of aqueous-SOA in the dryer element.

2.3.3 Estimation of Aerosol Liquid Water Content (LWC)

Aerosol LWC includes water associated with inorganic aerosol and OA, which were calculated using a thermodynamic model and an empirical method, respectively. Inorganic LWC (W_i) in mol L^{-1} was predicted by ISORROPIA-II in forward mode (Fountoukis and Nenes, 2007). Inputs for ISORROPIA-II include inorganic aerosol mass concentrations (SO_4^{2-}, inorganic NO_3^-, and NH_4^+) and meteorological parameters (temperature and RH). Calculation empirical of organic LWC (W_O) follows (Petters and Kreidenweis, 2007; Guo et al., 2015):

$$W_O = \frac{m_{org}\rho_w}{\rho_{org}} \frac{\kappa_{org}}{(1/RH - 1)} \quad (9)$$

where m_{org} is the organic mass concentration (μg m^{-3}) and ρ_w is the density of water (1 g cm^{-3}). The organic density (ρ_{org}, g cm^{-3}) was estimated using an empirical equation based on elemental ratios (Kuwata et al., 2012; Guo et al., 2015):

$$\rho_{org} = 1000 \times \left[\frac{12+\frac{H}{C}+16\times\frac{O}{C}}{7.0+5\times\frac{H}{C}+4.15\times\frac{O}{C}}\right] \quad (10)$$

The hygroscopicity of SOA generated during chamber studies under sub-saturated regimes depends on the OA degree of oxidation (Prenni et al., 2007; Jimenez et al., 2009; Petters et al., 2009; Chang et al., 2010). A simple linear relationship between the OA degree of oxidation (defined as the fraction of the total signal at *m/z* 44, f_{44}) and hygroscopicity (κ_{org}) is used (Duplissy et al., 2011):

$$\kappa_{org} = 2.2 \times f_{44} - 0.13 \quad (11)$$

The total LWC is then found by summing the water content associated with each mass fraction:

$$LWC = W_i + W_O \quad (12)$$

3 Results and Discussion

3.1 Temporal Dependences of Submicron Aerosol Composition

Campaign overview data for winter and summer are shown in Table 1 and Fig. 1. This includes meteorological parameters (e.g., temperature, RH, radiometer, precipitation, wind direction and speed), trace gases (e.g., CO, SO_2, NO_2, and O_3), and chemically resolved NR-PM_1 concentrations.

Data indicate that the average concentration of NR-PM_1 during winter campaign was 6.0 ±

293 3.7 μg m^{-3}, ranging from 0.5 to 14.8 μg m^{-3}. Mass loadings of NR-PM_1 at this measurement site
294 are relatively smaller than at a site near the HSC in winter 2015 (10.8 μg m^{-3} (Wallace et al.,
295 2018)), perhaps suggesting a weaker industrial influence at the UHSL site.

296 The average concentration of NR-PM_1 during summer was 3.6 ± 1.7 μg m^{-3}, ranging from
297 0.3 to 13.7 μg m^{-3}. For comparison, a summer campaign in 2006 on an elevated building near
298 downtown Houston showed an average NR-PM_1 concentration of approximately 11 μg m^{-3}
299 (Cleveland et al., 2012). An elevated NR-PM_1 episode was observed from May 28-31 (Fig.
300 1(j)), with high solar radiation and O_x ($O_x = NO_2 + O_3$) levels during the daytime, and high RH
301 at night, resulting in OA becoming the largest fractional species, likely due to gas-phase
302 photochemical production of SOA together with the nighttime increase of SOA associated with
303 high RH, lowered boundary layer and cooler temperatures.

304 In winter, OA was the largest component of NR-PM_1, accounting for 38 ± 13% on average
305 of the total mass, followed by SO_4^{2-} (23 ± 11%), NO_3^- (23 ± 11%), NH_4^+ (15 ± 5%) and Cl^- (1 ±
306 0.2%) (Fig. 2). Primary OA (POA=HOA+BBOA+COA) was responsible for 61 ± 19% of OA
307 mass. Secondary species (SO_4^{2-}+NO_3^-+NH_4^++LO-OOA+MO-OOA) accounted for ~76 ± 21%
308 of NR-PM_1 mass, which is higher than that in winter in Seoul (Kim et al., 2017) and Beijing
309 (Hu et al., 2016).

310 In contrast to winter, OA during the summer campaign constituted on average 47 ± 18% of
311 NR-PM_1 mass, and SO_4^{2-} was the second largest component (36 ± 15%), followed by NH_4^+ (14
312 ± 5%). NO_3^- only accounted for 2 ± 1% of NR-PM_1 mass in the summer, and Cl^- contributed 1
313 ± 0.5% of NR-PM_1 mass. The increased planetary boundary layer (PBL) height in summer
314 (Haman et al., 2012) likely contributed to relatively lower trace gas and NR-PM_1 levels in the

315 summer. Secondary species contributed ~88 ± 15% of NR-PM_1 mass, indicating that the
316 relative importance of secondary aerosol formation increased during summer as compared to
317 winter, especially for species such as SO_4^{2-} and MO-OOA.

318 The total OA displayed high values during the nighttime hours in both winter and summer,
319 maintaining a high level until morning rush hour, and then decreasing to a minimum value after
320 9:00 (Fig. 3). The summertime OA presented a small peak at noon, suggesting that
321 photochemical formation of OA played a more important role in summer than in winter.
322 Increasing ambient temperature and PBL height after sunrise causes re-partitioning to the gas
323 phase, likely contributing to the decrease of OA, LO-OOA and ON during daytime.

324 Contributions of PMF factors to wintertime and summertime OA show significant
325 differences. For wintertime OA, on average, BBOA contributed to 26% of OA mass; MO-OOA
326 and COA made the same contributions of 22% to total OA mass. The LO-OOA accounted for
327 17% of OA mass, followed by HOA (13%). The POA constituted more than half of OA mass
328 (61%), with the remainder of being OOA (39%). In the summer, LO-OOA represented the
329 largest fraction of the OA mass (54% on average), followed by MO-OOA (23%), HOA (15%)
330 and BBOA (8%). In the case of summer, OOA constituted 77% of OA and 36% of total
331 NR-PM_1 mass, which are almost two times their relative contributions in winter. The time
332 series of mass concentrations of NR-PM_1 species (Fig. 1) and OA factors (Fig. 4) in summer
333 were relatively stable and repeatable, while they varied dramatically in winter due to the
334 different meteorological conditions.

335

336 **3.2 Seasonal Variation of the Formation of Sulfate and Nitrate**

During the summer campaign, the prevailing southerly winds from the Gulf of Mexico carry marine aerosols to Houston (Schulze et al., 2018), resulting in a relatively high fraction of SO_4^{2-} and MSA. As shown in Fig. 1(g, j), the increased contribution of SO_4^{2-} occurred when winds originated from the south at a high speed (e.g., May 16-27), while the contribution of SO_4^{2-} decreased significantly when winds originated from the north (e.g., May 10th and May 13-15). MSA was markedly elevated during periods of southerly winds (Fig. S2(F)), and O/C and OM/OC were relatively higher (Fig. S2(D)). In addition, elevated SO_2 plumes were recorded during periods of southerly winds (Fig. 1(g, h)), potentially as a result of emissions from the Parish coal-fired power plant. In contrast to SO_4^{2-}, the fractional contribution of NO_3^- and OA increased greatly when the winds were not southerly. Primary pollutants such as CO and NO_2, were elevated when winds were northerly (Fig. 1(h)), accompanied by lower O/C and higher H/C ratios during the corresponding periods (Fig. S2(D), e.g., May 1st, 2rd, 10th, 15th).

Diurnal patterns of NR-PM_1 and other species in the winter and summer (Fig. 3) suggest significant seasonal dependence of sources and formation processes of NR-PM_1 species in Houston. In the case of SO_4^{2-}, the diurnal pattern displayed a daytime peak in both winter and summer, with the peak much more pronounced in summer mid-day. In winter, the f_{SO4} (mole ratio of $[SO_4^{2-}]$ to the sum of $[SO_2]$ and $[SO_4^{2-}]$) and LWC have concurrent peak values during the night time. However, there is no obvious correlation between f_{SO4} and LWC in summer, though a moderate correlation (r = 0.44) was found in winter. These results suggest that SO_4^{2-} formed though aqueous-phase chemistry in winter is more prominent than that in summer.

The total nitrate concentration was higher in winter than in summer. The NO_3^-,$_{AN}$ was very low in summer due to its thermal instability under high temperature, while it was relatively

enhanced in winter. According to the NO_x^+ ratio method described in Sec. 2.3.1, the mass fraction of NO_3^-,AN in total nitrate was in the range of 65-66% in winter, and in the range of 19-39% in summer. The averaged bound concentrations of NO_3,ON ranged from 0.22-0.34 μg m^{-3} in winter, and 0.05-0.06 μg m^{-3} in summer. The seasonal variation of NO_3^-,AN is much stronger than that of NO_3,ON. This is in accordance with previous observations in Atlanta, Georgia and Centreville, Alabama (Xu et al., 2015).

The diurnal profiles of NO_3,ON show that it reached peak value before dawn in both seasons (Fig. 5). However, NO_3^-,AN presents a bimodal diurnal profile in both seasons. The NO_3^-,AN, which increased from late afternoon and peaked at 2:00-4:00, was likely formed through nighttime chemistry from dinitrogen pentoxide (N_2O_5) hydrolysis, as the LWC displayed a trend similar to that of NO_3^-,AN, This was corroborated by the observation of O_x (>25 ppb), which is needed to form N_2O_5 (via $NO_3^\cdot$). The second peak observed during morning rush hour was likely formed though photochemical processing of NO_x emitted from vehicles because the traffic flow and O_x level are elevated during morning rush hour. The decreasing trend of NO_3^-,AN after 9:00 is presumed to be a result of enhanced PBL height and evaporation.

The estimated ON accounted for 4-8% of the total NR-PM_1 and 9-17% percent of the OA in summer and 12-27% of the total NR-PM_1 and 31-66% percent of the OA in winter, comparable to other studies (Fry et al., 2009; Rollins et al., 2010; Xu et al., 2015; Berkemeier et al., 2016). A proxy for $NO_3^\cdot$ production rate is based on the product of the observations of [NO_2] and [O_3] (Rollins et al., 2012), where brackets represent mixing ratios in ppb. The O_x (> 25 ppb) and elevated NO_x observed at night in summer (Fig. 3) resulted in rapid $NO_3^\cdot$ formation. Thus, the concurrent enhancement in ON and O_3 times NO_2 occurring during

nighttime (Fig. S4) presumably was caused by the nocturnal $NO_3^{\cdot}$-initiated oxidation of anthropogenic and biogenic VOCs, with the latter probably larger than the former (Brown et al., 2013). The high N/C ratio of LO-OOA, concurrent peak value in LO-OOA and ON (MW=231 g mol^{-1}) during nighttime hours (Fig. 3), and appreciable correlation of LO-OOA and ON in summer (r = 0.73) (Fig. 4) together suggest that particle-phase ON from $NO_3^{\cdot}$-initiated chemistry contributed to nighttime LO-OOA in summer.

3.3 Effects of Aqueous-phase and Photochemical Oxidation on OOA Formation

On average, OOA accounted for 39 ± 19% of OA mass in winter but increased to 77 ± 16% in summer. Note that MO-OOA accounted for more than half of OOA in winter (56%), indicating the more important role of MO-OOA in winter as compared to LO-OOA on a relative basis. In contrast, LO-OOA dominated OOA in summer (70%). The mass spectra of MO-OOA in winter and summer are similar (Fig. 6, r = 0.84) as are the extent of oxidation (O/C = 1.10 versus 1.07). However, LO-OOA in winter showed a different spectral pattern compared with that in summer. The mass spectrum of LO-OOA in winter was characterized by high *m/z* 32 (mainly CH_4O^+) and 46 (mainly $CH_2O_2^+$) peaks, resulting in a relatively high O/C (0.89) in winter that suggest LO-OOA in winter was more aged than that in summer (O/C=0.74).

Sun et al. (2016) reported a unique OOA in ambient air, termed aq-OOA (aqueous-phase-processed SOA), that strongly correlated with particle LWC, sulfate and S-containing ions. As shown in Table 2, by comparing the mass spectra of OOA in this work with aq-OOA, it is found that the mass spectra of MO-OOA in winter in this study presents a

much stronger correlation (r =0.96) with aq-OOA, rather than LO-OOA in winter in this study (r =0.75). Both MO-OOA and LO-OOA in summer highly correlated with aq-OOA. This result indicates that the formation of LO-OOA in summer and MO-OOA in both seasons may involve aqueous-phase chemistry.

Assuming that OOA deduced from PMF analysis can be used as a surrogate of SOA (Wood et al., 2010; Xu et al., 2017), the two OOA were used to investigate the formation mechanisms and evolutionary processes of SOA. Previous studies have found SOA correlated well with odd oxygen (O_x) in many cities (Wood et al., 2010; Sun et al., 2011; Hayes et al., 2013; Zhang et al., 2015; Xu et al., 2017) and that SOA formation is significantly impacted by aqueous-phase processing (Lim et al., 2010; Ervens et al., 2011; Xu et al., 2017). The relationships between OOA factors and O_x/LWC were used as the metrics to characterize SOA formation mechanisms associated with photochemistry/aqueous oxidation chemistry (Xu et al., 2017).

Fig. 7 (A, B) indicates the LWC frequency distribution. Winter LWC are binned in 5 μg m^{-3} increments from 0 to 20 μg m^{-3}. Data in the ranges of 20 to 30 μg m^{-3}, 30 to 50 μg m^{-3}, 50 to 80 μg m^{-3}, and 80 to 120 μg m^{-3} are shown as 25, 40, 65 and 100 μg m^{-3}, respectively. Summer LWC are binned in 2.5 μg m^{-3} increments from 0 to 15 μg m^{-3}. The bins shown as 17.5 and 27.5 μg m^{-3} represent data from 15 to 20 μg m^{-3} and 20 to 35 μg m^{-3}. It should be noted that a fit for the binned data likely results in an increase in R^2 compared to the fit for the original data.

The data associated with the artificially created bins in both seasons did not pass the normal test and homogeneity test of variances. The statistical significance of differences between bins was then tested using the Kruskal-Wallis analysis of variance (K-W ANOVA).

425 The differences between winter and summer data of the bins were significant. Thus, the
426 Dunn-Bonferroni test was performed for the *post-hoc* pairwise comparisons. It was found that
427 the difference of all measured variables in different bins shown in Fig. 7 were significant
428 (p<0.01). The results can be found in Tables S6-S7. Fig. 7(C, D) presents a clear positive trend
429 of RH as a function of LWC in both winter and summer which implies an increased potential
430 for aqueous-phase processing at high RH level, enhanced by low wind speed that allows
431 accumulation of pollutants (Fig. 7(E, F)). The patterns of other parameters as LWC increases in
432 winter were different from those in summer.

433 The variation of binned mean OA mass against LWC presents significant seasonal
434 difference (Fig. 7(A, B)). In winter, the OA mass increased when LWC increased from 2.5 to
435 12.5 μg m^{-3} but decreased as the LWC increased further. The LO-OOA mass decreased
436 dramatically when LWC>12.5 μg m^{-3} (RH>80%, Fig. 7(C)) while MO-OOA continues
437 increasing until LWC> 40 μg m^{-3}. This result indicates that wet removal may dominate under
438 an extremely high RH environment coupled with stagnant air (WS <2 m/s Fig. 7(E)), as the OA
439 concentration decreased at extremely high LWC level (Fig. 7(A)). In summer, the OA mass
440 decreased when LWC increased from 1.25 to 6.25 μg m^{-3} but increased when LWC increased
441 further, suggesting the wet removal effect is not as strong as that in winter because of the
442 relatively lower LWC in summer.

443 On average, LO-OOA (Fig. 7(G, H)) in winter increased from 0.3 to 0.9 μg m^{-3} when LWC
444 increased from 2.5 to 7.5 μg m^{-3} but decreased as the LWC increased further, particularly when
445 LWC >40 μg m^{-3}. The slope of this decrease was approximately -0.008 μg LO-OOA μg^{-1} LWC.
446 Fig. 7(A) shows that 64% of the data points were observed in the situation of low LWC (<12.5

447 μg m^{-3}, RH<80%), when the increase of LO-OOA was more significant than that of MO-OOA.
448 In contrast, LO-OOA in summer showed a decreasing trend under low LWC level (LWC<6.25
449 μg m^{-3}, RH<80%) but an increasing trend from approximately 0.77 μm^{-3} to 1.8 μg m^{-3} as LWC
450 increased from 6.25 to 27.5 μg m^{-3}, a slope of 0.053 μg LO-OOA μg^{-1} LWC. The relatively
451 high LO-OOA under low LWC level was likely more regional, with contributions from
452 possibly transported non-aqueous OOA, as the wind speed in this case was relatively high and
453 RH was low. The formation of LO-OOA under high LWC level was likely enhanced by local
454 aqueous-phase heterogeneous chemistry.

455 MO-OOA (Fig. 7(I, J)) slightly increased during both seasons as LWC increased. In winter,
456 MO-OOA presented a similar increasing trend from 0.57 to 0.98 μg m^{-3} when LWC increased
457 from 2.5 to 40 μg m^{-3} but decreased as the LWC increased further. The slope of this increase
458 was approximately 0.008 μg MO-OOA μg^{-1} LWC. In summer, MO-OOA appears to increase
459 from 0.49 to 0.64 μg m^{-3} when LWC increased from 2.5 to 27.5 μg m^{-3}, with slope of 0.005 μg
460 MO-OOA μg^{-1} LWC. In winter, because of the decrease in LO-OOA with LWC, the relative
461 fraction of MO-OOA increases as LWC increases.

462 The mutual effect of aqueous-phase and photochemistry on OOA formation prevents solely
463 evaluating the role of the two processes. Sullivan et al. (2016) reported multiple lines of
464 evidence for local aq-SOA formation observed in the Po Valley, Italy during times of increasing
465 RH, which coincided with dark conditions. Thus, the daytime data were separated to examine
466 the variation of OOA against O_x. The relationship between OOA and aqueous-phase chemistry
467 was investigated further by excluding the daytime data, with the aim of diminishing the
468 influence of photochemistry. To do so, nighttime and daytime were based on sunrise and sunset

469 in Houston during the two campaigns (https://www.timeanddate.com/sun/usa/houston). On
470 average, the day lengths are 11 h 10 min and 13 h 35 min for the campaigns in February and
471 May, 2014, respectively.

472 The potential linear relationship between OOA and LWC for the nighttime data was
473 investigated by fitting the data with a locally weighted scatter plot smoothing algorithm
474 (LOWESS, (Cleveland, 1981)). According to the LOWESS curves for the original nighttime
475 data and the resampled data obtained by a bootstrap method (Figs. S14-15), there likely exists a
476 linear relationship between LO-OOA and LWC for data points with LWC less than 20 μg m^{-3}
477 and greater than 6 μg m^{-3} for the winter and summer periods, respectively. As for MO-OOA,
478 such a linear relationship likely exists when LWC is less than 50 and 7 μg m^{-3} for the winter
479 and summer periods, respectively.

480 Figure 8 presents the scatter plots of OOA versus LWC during nighttime for the two
481 campaigns. The green dots denote the increasing trend of OOA against LWC. It is found that
482 the increase of wintertime LO-OOA under low LWC level (<20 μg m^{-3}) during the night is
483 stronger than that shown in Fig. 7 (G). The nighttime LO-OOA linearly increased from 0.04 to
484 0.64 μg m^{-3} when LWC increased from 2.5 to 17.5 μg m^{-3}, a slope of 0.033 μg LO-OOA μg^{-1}
485 LWC. This result indicates that the nighttime increase in LO-OOA in winter is more likely
486 formed via aqueous-phase chemistry in aerosol liquid water. The increase of LO-OOA under
487 high LWC level (LWC>6.25 μg m^{-3}) in summer during nighttime (0.055 μg LO-OOA μg^{-1}
488 LWC) was comparable to the increase rate of whole dataset (0.053 μg LO-OOA μg^{-1} LWC).
489 The slope of nighttime increase of MO-OOA against LWC during the winter campaign was
490 0.013 μg MO-OOA μg^{-1} LWC, which is 1.7 times the slope for the whole dataset (daytime and

491 nighttime). For the summer campaign, the increase of nighttime MO-OOA is 2.2 times the rate
492 for the whole dataset.

493 These results suggest that aqueous-phase processing likely has a strong positive impact on
494 the formation of MO-OOA in the two seasons except for instances when LWC exceeds 100 μg
495 m^{-3} in winter. It also appears to facilitate the local formation of LO-OOA under low LWC level
496 (<17.5 μg m^{-3}) in winter and under relatively high LWC level (>6.25 μg m^{-3}) in summer.

497 As mentioned previously, ON contributes significantly to summertime LO-OOA, and the
498 concurrent enhancement in ON and LO-OOA during night was associated with elevated RH
499 (Fig. 3). A previous study found that the partitioning of organic compounds to the particle phase
500 was significantly increased at elevated RH levels (70%) in an urban area dominated by
501 biogenic emissions in Atlanta (Hennigan et al., 2008). The correlation of ON and LO-OOA in
502 summer nighttime (r=0.76) was stronger than that during daytime (r =0.53). Thus, we presume
503 that aerosol water facilitates the formation of ON from NO_3˙-initiated chemistry involving
504 BVOCs during nighttime, resulting in a good relationship of LO-OOA and LWC in summer.

505 MSA is a secondary product from the oxidation of dimethyl sulfide (Zorn et al., 2008),
506 which is a gaseous species emission from marine organisms (Barnes et al., 2006). Thus, MSA is
507 found to be abundant in marine/coastal areas and play an important role in the formation of
508 marine PM (Gondwe, et al., 2004; Huang et al., 2015; Schulze et al., 2018). The formation of
509 MSA is unique to aqueous-phase processing and could be used as an indicator of aqueous SOA
510 formation (Barnes et al., 2006; Ervens et al., 2011). Recent observations confirmed that MSA
511 and associated fragment ions ($CH_2O_2^+$ (m/z 46), $C_2O_2^+$ (m/z 56) and $C_2H_2O_2^+$ (m/z 58), which
512 are unique ions of glyoxal and methylglyoxal uptake on SOA (Chhabra et al., 2010)) strongly

513 correlated with SOA formed via aqueous-phase processing (Ge et al., 2012; Sun et al., 2016). In
514 this work, MO-OOA formation was associated with aqueous-phase oxidation more strongly
515 than LO-OOA in winter, which likely can be further verified by the correlations between
516 MO-OOA/LO-OOA and MSA. As shown in Fig. 6, MSA has a relatively higher correlation
517 coefficient with MO-OOA (r=0.45) compared to LO-OOA (r=0.30), though the correlation also
518 is influenced by many other factors.

519 Fig. 9(A, B) presents the frequency distribution of O_x. Winter O_x are binned in 10 ppb
520 increments from 0 to 60 ppb. The range for summer is 20 to 70 ppb. The data associated with
521 the artificially created O_x bins in both seasons did not pass the normal test and homogeneity test
522 of variances. The K-W ANOVA for winter and summer data of the bins were significant. The
523 Dunn-Bonferroni test for the *post-hoc* pairwise comparisons shows that the difference of
524 measured variables among different bins shown in Fig. 9 were significant (Tables S8-S9). The
525 clear positive relationship between solar radiation and O_x is shown in Fig. 9 (C, D), and the
526 negative relationship between solar radiation and RH is shown in Fig. 9 (E, F), suggesting
527 strong atmospheric photochemical activity associated with high O_x periods.

528 The variations of LO-OOA and MO-OOA showed substantially different patterns with
529 increases of O_x in winter and summer. In winter, LO-OOA and MO-OOA showed comparable
530 increasing trends at low O_x level (<35 ppb), with MO-OOA having a stronger response. The
531 LO-OOA was increased from 0.13 to 0.72 μg m^{-3} when O_x increased from 5 to 35 ppb but
532 decreased as the O_x increased further. The slope of this increase was approximately 0.023 μg
533 LO-OOA ppb^{-1} O_x. MO-OOA increased from 0.13 to 0.88 μg m^{-3} when the O_x increased from 5
534 to 35 ppb, with a slope of 0.027 μg MO-OOA ppb^{-1} O_x. This leads to a maximum in the mass

fraction of MO-OOA in the mid-O_x level range and also at highest levels of observed O_x.

In summer, there is a clear decreasing trend of RH with increases of O_x. As discussed previously, the high level of summertime LO-OOA likely was associated with high LWC. Therefore, the high mass fraction of LO-OOA at the lowest O_x level (<20 ppb) associated with the high RH/LWC was likely from aqueous-phase chemistry. After excluding low-O_x data (<20 ppb), LO-OOA showed a much stronger response to O_x than did MO-OOA. The summer LO-OOA increased from approximately 0.6 to 1.8 μg m^{-3} when O_x increased from 25 to 65 ppb, a slope of 0.03 μg LO-OOA ppb^{-1} O_x. This increase was likely in the case of low RH conditions (<80%, Fig. 7 (D)), when aqueous-phase chemistry did not promote the formation of LO-OOA (Fig. 7 (H)). Summer MO-OOA increased from 0.36 to 0.67 μg m^{-3} when O_x increased from 25 to 55 ppb but decreased as the O_x increased further. The slope of this increase was 0.007 μg MO-OOA ppb^{-1} O_x. Contrary to winter, LO-OOA responded more strongly to increases of O_x than MO-OOA did.

The relationship of OOA versus O_x was examined further by excluding nighttime data. According to the LOWESS curves for the original daytime data and the resampled data obtained using a bootstrap method (Figs. S16-17), there likely exists a linear relationship between LO-OOA and O_x when O_x is less than 35 ppb and greater than 20 ppb for the winter and summer period, respectively. As for MO-OOA, the linear relationship likely exists for data points with O_x less than 35 ppb for the winter period, but it is less prominent.

Figure 10 presents the scatter plots of daytime OOA versus O_x for the winter and summer campaign. The daytime responses of LO-OOA and MO-OOA to O_x in winter were ~1.5 times that for the whole dataset (Fig. 9 (G, I)), and the increase rate of MO-OOA was higher than that

of LO-OOA. In summer, the slope of the daytime increase of LO-OOA was 1.24 times that for the whole campaign (Fig. 10 (H)). These results suggest that the photochemical enhancement of OOA in winter was more prominent than that in summer. For the summer campaign, the formation of LO-OOA was more strongly linked to photochemistry compared to MO-OOA. At low atmospheric oxidative capacity (O_x<20 ppb), aqueous-phase chemistry was likely predominant in the formation of LO-OOA.

The combined effects of photochemistry and aqueous-phase chemistry on OOA composition during winter and summer are further demonstrated in Fig. 11. The ratio of MO-OOA/LO-OOA in winter showed the highest values on the left-top corner in Fig. 11 (A), suggesting photochemical processing was likely responsible for MO-OOA formation, under low LWC levels (< 10 μg m^{-3}). Additionally, data with high MO-OOA/LO-OOA on the right-bottom corner in Fig. 11 (A) indicate the important role of aqueous-phase chemistry under low O_x and high LWC levels. Overall, the concentration of MO-OOA in winter increased as O_x/LWC increased, whereas LO-OOA markedly decreased. This result indicates both photochemical and aqueous-phase processing played a more important role in enhancing MO-OOA than LO-OOA in winter. Furthermore, the diurnal patterns of wintertime LO-OOA only presented a peak value at night while MO-OOA showed one peak value at night (high LWC) and another one in the afternoon (high O_x period) (Fig. 3).

In summer, data points with low MO-OOA/LO-OOA value on the left-top of Figure 11 (B) illustrated that LO-OOA was enhanced in high-O_x and low-LWC conditions, though the low MO-OOA/LO-OOA values are not confined to just the top left. In case of high LWC level (LWC> 6.5 μg m^{-3}), MO-OOA/LO-OOA were much lower (on the right of Figure 11 (B),

579 particularly when LWC> 10 μg m^{-3}). Although MO-OOA increased with LWC and O_x, the
580 increase of LO-OOA was more significant. The effects of both photochemistry (≥ 25 ppb) and
581 aqueous-phase chemistry (≥ 6.5 μg m^{-3}) were more relevant for the formation of LO-OOA than
582 MO-OOA. On average, the mass concentration of LO-OOA was elevated by nearly 1.2 μg m^{-3}
583 as a ~20 μg change in LWC (increased from 6.25 μg m^{-3} to 27.5 μg m^{-3}, Fig. 7 (H)), which is
584 equivalent to a 40 ppb change in O_x (increased from 25 ppb to 65 ppb, Fig. 9 (H)). This result
585 further suggests that the aqueous-phase chemistry is comparable to photochemistry in
586 processing LO-OOA in summer. The diurnal pattern of summertime LO-OOA displays a peak
587 value at night and a comparable peak value in the afternoon (Fig. 3).
588

589 ## 4 Conclusions

590 Seasonal characterization of NR-PM_1 collected using HR-ToF-AMS near Houston in 2014
591 demonstrated that the mass loading, diurnal patterns, and important formation pathways of
592 NR-PM_1 vary seasonally. The OA was the largest component of NR-PM_1 mass, on average,
593 accounting for 38% and 47% of the mass loadings in winter and summer, respectively, which is
594 less than that in the north part of Houston, which is influenced by high biogenic emission rates.
595 Nitrate was the second largest component in winter (23%) but accounted for only 2% of
596 NR-PM_1 mass in summer; SO_4^{2-} was the second largest component in winter (23%) and
597 summer (36%), respectively. ON, on average accounted for 31-66 and 9-17 % of OA during
598 winter and summer campaign, respectively. The summertime ON correlated very well with
599 LO-OOA and concurrently peaked at nighttime. It is likely that ON from $NO_3^{\bullet}$-initiated
600 oxidation of BVOC in the forested northeastern Houston contributed greatly to nighttime

601 LO-OOA in summer.

602 Contributions of factors to wintertime and summertime OA show distinct differences. For
603 wintertime OA, on average, BBOA contributed 26% of OA mass, and MO-OOA and COA
604 made the same contribution of 22% to total OA mass. LO-OOA accounted for 17% of OA mass,
605 followed by HOA (13%). In the summer, LO-OOA represented the largest fraction of the OA
606 mass, 54% on average. The second largest contributor was MO-OOA (23%). Together, POA
607 constituted more than half of OA mass (61%) in winter, while it accounted for 23% of OA mass
608 in summer, highlighting the enhanced impact of primary emissions on OA level during
609 wintertime. Secondary aerosols account for ~76% and 88% of NR-PM_1 mass in winter and
610 summer, respectively, indicating NR-PM_1 mass was likely driven mostly by secondary aerosol
611 formation.

612 The two proxies of SOA (LO-OOA and MO-OOA) presented seasonal differences in their
613 spectral patterns, oxidation degrees and contributions to SOA. MO-OOA showed a higher
614 contribution to SOA than LO-OOA in winter (56% vs. 44%). In contrast, LO-OOA dominated
615 SOA in summer (70%). Our results indicate that both photochemical and aqueous-phase
616 chemistry played important roles in the formation of MO-OOA and LO-OOA. Aqueous-phase
617 processing likely has strong positive impact on the formation of MO-OOA in the two seasons,
618 especially in winter. The relationships between MO-OOA and LWC were 0.008 and 0.005 μg
619 MO-OOA μg^{-1} LWC during winter and summer, respectively. Wet removal likely limits
620 MO-OOA when LWC exceeds 100 μg m^{-3} in winter. The relative importance of aqueous-phase
621 chemistry versus photochemistry in processing LO-OOA was dependent on RH.
622 Aqueous-phase processing likely facilitated the local formation of wintertime LO-OOA at low

LWC level (<17.5 μg m^{-3}, RH<80%), with a stronger dependence (0.033 μg LO-OOA $μg^{-1}$ LWC) than MO-OOA. In summer, the formation of LO-OOA was enhanced by aqueous-phase processing at relatively high LWC level (>6.25 μg m^{-3}, RH>80%) with a slope of 0.053 μg LO-OOA $μg^{-1}$ LWC, while LO-OOA was likely transported non-aqueous regional OOA when LWC < 6.25 μg m^{-3}. These increases of OOA in response to LWC were greatly enhanced during nighttime. Aqueous-phase chemistry also was predominant in the formation of summertime LO-OOA at low atmospheric oxidative capacity (O_x < 20 ppb). In general, summertime LO-OOA showed a much stronger response to O_x than did MO-OOA, with a slope of 0.030 μg LO-OOA ppb^{-1} O_x. LO-OOA in summer was elevated by nearly 1.2 μg m^{-3} as a ~20 μg change in LWC, which is equivalent to a 40 ppb change in O_x.

Acknowledgments

The authors would like to acknowledge Yele Sun (Institute of Atmospheric Physics, Chinese Academy of Sciences) for providing the aq-OOA mass spectra, and Qiao Zhu (Peking University Shenzhen Graduate School) for assistance in the calculation of organic nitrates and PMF analysis. The scholarships provided by China Scholarship Council to Qili Dai and Xiaohui Bi are gratefully acknowledged. Support of the Houston Endowment in development and deployment of the MAQL also is gratefully acknowledged. Datasets are available by contacting the corresponding author.

Author contribution. Qili Dai performed the data analysis and wrote the manuscript. Robert J. Griffin and Yinchang Feng assisted heavily with manuscript development and editing. Henry W. Wallace, Alexander A.T. Bui, James H. Flynn, and Barry L. Lefer contributed to data collection during the field campaigns. Benjamin C. Schulze, Henry W. Wallace, Alexander A.T. Bui and Nancy P. Sanchez contributed with data analysis. Xiaohui Bi, Benjamin C. Schulze, Alexander A.T. Bui, Fangzhou Guo, Nancy P. Sanchez, and James H. Flynn provided helpful comments and edits.

Competing interests. The authors declare that they have no conflict of interest.

References

Allen, D. T., and Fraser, M.: An overview of the Gulf Coast Aerosol Research and Characterization Study: The Houston Fine Particulate Matter Supersite, J. Air Waste Manage., 56, 456-466, http://doi.org/10.1080/10473289.2006.10464514, 2006.

Atkinson, D. B., Massoli, P., O'Neill, N. T., Quinn, P. K., Brooks, S. D., and Lefer, B.: Comparison of in situ and columnar aerosol spectral measurements during TexAQS-GoMACCS 2006: testing parameterizations for estimating aerosol fine mode properties, Atmos. Chem. Phys., 10, 51-61, http://doi.org/10.5194/acp-10-51-2010, 2010.

Ayres, B. R., Allen, H. M., Draper, D. C., Brown, S. S., Wild, R. J., Jimenez, J. L., Day, D. A., Campuzano-Jost, P., Hu, W., de Gouw, J., Koss, A., Cohen, R. C., Duffey, K. C., Romer, P., Baumann, K., Edgerton, E., Takahama, S., Thornton, J. A., Lee, B. H., Lopez-Hilfiker, F. D., Mohr, C., Wennberg, P. O., Nguyen, T. B., Teng, A., Goldstein, A. H., Olson, K., and Fry, J. L.: Organic nitrate aerosol formation via NO_3 + biogenic volatile organic compounds in the southeastern United States, Atmos. Chem. Phys., 15, 13377-13392, http://doi.org/10.5194/acp-15-13377-2015, 2015.

Bahreini, R., Ervens, B., Middlebrook, A. M., Warneke, C., de Gouw, J. A., DeCarlo, P. F., Jimenez, J. L., Brock, C. A., Neuman, J. A., Ryerson, T. B., Stark, H., Atlas, E., Brioude, J.,

Fried, A., Holloway, J. S., Peischl, J., Richter, D., Walega, J., Weibring, P., Wollny, A. G., and Fehsenfeld, F. C.: Organic aerosol formation in urban and industrial plumes near Houston and Dallas, Texas, J. Geophys. Res., 114, D00f16, http://doi.org/10.1029/2008jd011493, 2009.

Barnes, I., Hjorth, J., and Mihalopoulos, N.: Dimethyl sulfide and dimethyl sulfoxide and their oxidation in the atmosphere, Chem. Rev., 106, 940-975, http://doi.org/10.1021/cr020529+, 2006.

Bates, T. S., Quinn, P. K., Coffman, D., Schulz, K., Covert, D. S., Johnson, J. E., Williams, E. J., Lerner, B. M., Angevine, W. M., Tucker, S. C., Brewer, W. A., and Stohl, A.: Boundary layer aerosol chemistry during TexAQS/GoMACCS 2006: Insights into aerosol sources and transformation processes, J. Geophys. Res., 113, D00f01, http://doi.org/10.1029/2008jd010023, 2008.

Bean, J. K., Faxon, C. B., Leong, Y. J., Wallace, H. W., Cevik, B. K., Ortiz, S., Canagaratna, M. R., Usenko, S., Sheesley, R. J., Griffin, R. J., and Hildebrandt, L: Composition and sources of particulate matter measured near Houston, TX; Anthropogenic-biogenic interactions, Atmos., 7, 73, https://doi.org/10.3390/atmos7050073, 2016

Berkemeier, T., Ammann, M., Mentel, T. F., Poschl, U., and Shiraiwa, M.: Organic Nitrate Contribution to New Particle Formation and Growth in Secondary Organic Aerosols from alpha-Pinene Ozonolysis, Environ. Sci. Technol., 50, 6334-6342, http://doi.org/10.1021/acs.est.6b00961, 2016.

Boyd, C. M., Sanchez, J., Xu, L., Eugene, A. J., Nah, T., Tuet, W. Y., Guzman, M. I., and Ng, N. L.: Secondary Organic Aerosol (SOA) formation from the β-pinene CNO3 system: effect of humidity and peroxy radical fate, Atmos. Chem. Phys., 15, 7497–7522, doi:10.5194/acp-15-7497-2015, 2015.

Brown, S. S., Dube, W. P., Bahreini, R., Middlebrook, A. M., Brock, C. A., Warneke, C., de Gouw, J. A., Washenfelder, R. A., Atlas, E., Peischl, J., Ryerson, T. B., Holloway, J. S., Schwarz, J. P., Spackman, R., Trainer, M., Parrish, D. D., Fehshenfeld, F. C., and Ravishankara, A. R.: Biogenic VOC oxidation and organic aerosol formation in an urban nocturnal boundary layer: aircraft vertical profiles in Houston, TX, Atmos. Chem. Phys., 13, 11317-11337, http://doi.org/10.5194/acp-13-11317-2013, 2013.

Bruns, E. A., Perraud, V., Zelenyuk, A., Ezell, M. J., Johnson, S. N., Yu, Y., Imre, D., Finlayson-Pitts, B. J., and Alexander, M. L.: Comparison of FTIR and Particle Mass

Spectrometry for the Measurement of Particulate Organic Nitrates, Environ. Sci. Technol., 44, 1056–1061, 2010.

Canagaratna, M. R., Jayne, J. T., Jimenez, J. L., Allan, J. D., Alfarra, M. R., Zhang, Q., Onasch, T. B., Drewnick, F., Coe, H., Middlebrook, A., Delia, A., Williams, L. R., Trimborn, A. M., Northway, M. J., DeCarlo, P. F., Kolb, C. E., Davidovits, P., and Worsnop, D. R.: Chemical and microphysical characterization of ambient aerosols with the aerodyne aerosol mass spectrometer, Mass Spectrom. Rev., 26, 185-222, http://doi.org/10.1002/mas.20115, 2007.

Canagaratna, M. R., Jimenez, J. L., Kroll, J. H., Chen, Q., Kessler, S. H., Massoli, P., Hildebrandt Ruiz, L., Fortner, E., Williams, L. R., Wilson, K. R., Surratt, J. D., Donahue, N. M., Jayne, J. T., and Worsnop, D. R.: Elemental ratio measurements of organic compounds using aerosol mass spectrometry: characterization, improved calibration, and implications, Atmos. Chem. Phys., 15, 253-272, http://doi.org/10.5194/acp-15-253-2015, 2015.

Chang, R. Y. W., Slowik, J. G., Shantz, N. C., Vlasenko, A., Liggio, J., Sjostedt, S. J., Leaitch, W. R., and Abbatt, J. P. D.: The hygroscopicity parameter (kappa) of ambient organic aerosol at a field site subject to biogenic and anthropogenic influences: relationship to degree of aerosol oxidation, Atmos. Chem. Phys., 10, 5047-5064, http://doi.org/10.5194/acp-10-5047-2010, 2010.

Chhabra, P. S., Flagan, R. C., and Seinfeld, J. H.: Elemental analysis of chamber organic aerosol using an aerodyne high-resolution aerosol mass spectrometer, Atmos. Chem. Phys., 10, 4111-4131, http://doi.org/10.5194/acp-10-4111-2010, 2010.

Cleveland, M. J., Ziemba, L. D., Griffin, R. J., Dibb, J. E., Anderson, C. H., Lefer, B., and Rappengluck, B.: Characterization of urban aerosol using aerosol mass spectrometry and proton nuclear magnetic resonance spectroscopy, Atmos. Environ., 54, 511-518, http://doi.org/10.1016/j.atmosenv.2012.02.074, 2012.

Cleveland, W. S. (1981) LOWESS: A program for smoothing scatterplots by robust locally weighted regression. Am. Stat., 35, 54.

Crippa, M., El Haddad, I., Slowik, J. G., DeCarlo, P. F., Mohr, C., Heringa, M. F., Chirico, R., Marchand, N., Sciare, J., Baltensperger, U., and Prevot, A. S. H.: Identification of marine and continental aerosol sources in Paris using high resolution aerosol mass spectrometry, J. Geophys. Res., 118, 1950-1963, http://doi.org/10.1002/jgrd.50151, 2013.

DeCarlo, P. F., Kimmel, J. R., Trimborn, A., Northway, M. J., Jayne, J. T., Aiken, A. C., Gonin, M., Fuhrer, K., Horvath, T., Docherty, K. S., Worsnop, D. R., and Jimenez, J. L.: Field-deployable, high-resolution, time-of-flight aerosol mass spectrometer, Anal. Chem.,

78, 8281-8289, http://doi.org/10.1021/ac061249n, 2006.

Duplissy, J., DeCarlo, P. F., Dommen, J., Alfarra, M. R., Metzger, A., Barmpadimos, I., Prevot, A. S. H., Weingartner, E., Tritscher, T., Gysel, M., Aiken, A. C., Jimenez, J. L., Canagaratna, M. R., Worsnop, D. R., Collins, D. R., Tomlinson, J., and Baltensperger, U.: Relating hygroscopicity and composition of organic aerosol particulate matter, Atmos. Chem. Phys., 11, 1155-1165, http://doi.org/10.5194/acp-11-1155-2011, 2011.

El-Sayed, M. M. H., Amenumey, D., and Hennigan, C. J.: Drying-Induced Evaporation of Secondary Organic Aerosol during Summer, Environ Sci Technol, 50, 3626-3633, 10.1021/acs.est.5b06002, 2016.

Ervens, B., Turpin, B. J., and Weber, R. J.: Secondary organic aerosol formation in cloud droplets and aqueous particles (aqSOA): a review of laboratory, field and model studies, Atmos. Chem. Phys., 11, 11069-11102, http://doi.org/10.5194/acp-11-11069-2011, 2011.

Farmer, D. K., Matsunaga, A., Docherty, K. S., Surratt, J. D., Seinfeld, J. H., Ziemann, P. J., and Jimenez, J. L.: Response of an aerosol mass spectrometer to organonitrates and organosulfates and implications for atmospheric chemistry, P. Natl. Acad. Sci. USA, 107, 6670-6675, http://doi.org/10.1073/pnas.0912340107, 2010.

Fountoukis, C., and Nenes, A.: ISORROPIA II: a computationally efficient thermodynamic equilibrium model for K+-Ca2+-Mg2+-Nh(4)(+)-Na+-SO42--NO3--Cl--H2O aerosols, Atmos. Chem. Phys., 7, 4639-4659, , http://doi.org/10.5194/acp-7-4639-2007, 2007.

Fry, J. L., Kiendler-Scharr, A., Rollins, A. W., Wooldridge, P. J., Brown, S. S., Fuchs, H., Dube, W., Mensah, A., dal Maso, M., Tillmann, R., Dorn, H. P., Brauers, T., and Cohen, R. C.: Organic nitrate and secondary organic aerosol yield from NO3 oxidation of beta-pinene evaluated using a gas-phase kinetics/aerosol partitioning model, Atmos. Chem. Phys., 9, 1431-1449, http://doi.org/10.5194/acp-9-1431-2009, 2009.

Fry, J. L., Draper, D. C., Zarzana, K. J., Campuzano-Jost, P., Day, D. A., Jimenez, J. L., Brown, S. S., Cohen, R. C., Kaser, L., Hansel, A., Cappellin, L., Karl, T., Roux, A. H., Turnipseed, A., Cantrell, C., Lefer, B. L., and Grossberg, N.: Observations of gas- and aerosol-phase organic nitrates at BEACHON-RoMBAS 2011, Atmos. Chem. Phys., 13, 8585-8605, http://doi.org/10.5194/acp-13-8585-2013, 2013.

Ge, X., Zhang, Q., Sun, Y., Ruehl, C. R., and Setyan, A.: Effect of aqueous-phase processing on aerosol chemistry and size distributions in Fresno, California, during wintertime, Environ. Chem., 9, 221, http://doi.org/10.1071/en11168, 2012.

Gondwe, M., Krol, M., Klaassen, W., Gieskes, W., and de Baar, H.: Comparison of modeled

versus measured MSA:nss SO4= ratios: A global analysis, Global Biogeochem. Cy., 18, http://doi.org/10.1029/2003GB002144, 2004.

Grantz, D. A., Garner, J. H. B., and Johnson, D. W.: Ecological effects of particulate matter, Environ. Int., 29, 213-239, http://doi.org/10.1016/S0160-4120(02)00181-2, 2003.

Guo, H., Xu, L., Bougiatioti, A., Cerully, K. M., Capps, S. L., Hite, J. R., Carlton, A. G., Lee, S. H., Bergin, M. H., Ng, N. L., Nenes, A., and Weber, R. J.: Fine-particle water and pH in the southeastern United States, Atmos. Chem. Phys., 15, 5211-5228, http://doi.org/10.5194/acp-15-5211-2015, 2015.

Haman, C. L., Lefer, B., and Morris, G. A.: Seasonal Variability in the Diurnal Evolution of the Boundary Layer in a Near-Coastal Urban Environment, J. Atmos. Ocean Tech., 29, 697-710, , http://doi.org/10.1175/Jtech-D-11-00114.1, 2012.

Hayes, P. L., Ortega, A. M., Cubison, M. J., Froyd, K. D., Zhao, Y., Cliff, S. S., Hu, W. W., Toohey, D. W., Flynn, J. H., Lefer, B. L., Grossberg, N., Alvarez, S., Rappenglueck, B., Taylor, J. W., Allan, J. D., Holloway, J. S., Gilman, J. B., Kuster, W. C., De Gouw, J. A., Massoli, P., Zhang, X., Liu, J., Weber, R. J., Corrigan, A. L., Russell, L. M., Isaacman, G., Worton, D. R., Kreisberg, N. M., Goldstein, A. H., Thalman, R., Waxman, E. M., Volkamer, R., Lin, Y. H., Surratt, J. D., Kleindienst, E., Offenberg, J. H., Dusanter, S., Griffith, S., Stevens, P. S., Brioude, J., Angevine, W. M., and Jimenez, J. L.: Organic aerosol composition and sources in Pasadena, California, during the 2010 CalNex campaign, J. Geophys. Res., 118, 9233-9257, http://doi.org/10.1002/jgrd.50530, 2013.

Hennigan, C. J., Bergin, M. H., Dibb, J. E., and Weber, R. J.: Enhanced secondary organic aerosol formation due to water uptake by fine particles, Geophys. Res. Lett., 35, L18801, http://doi.org/10.1029/2008gl035046, 2008.

Hu, W. W., Campuzano-Jost, P., Palm, B. B., Day, D. A., Ortega, A. M., Hayes, P. L., Krechmer, J. E., Chen, Q., Kuwata, M., Liu, Y. J., de Sa, S. S., McKinney, K., Martin, S. T., Hu, M., Budisulistiorini, S. H., Riva, M., Surratt, J. D., St Clair, J. M., Isaacman-Van Wertz, G., Yee, L. D., Goldstein, A. H., Carbone, S., Brito, J., Artaxo, P., de Gouw, J. A., Koss, A., Wisthaler, A., Mikoviny, T., Karl, T., Kaser, L., Jud, W., Hansel, A., Docherty, K. S., Alexander, M. L., Robinson, N. H., Coe, H., Allan, J. D., Canagaratna, M. R., Paulot, F., and Jimenez, J. L.: Characterization of a real-time tracer for isoprene epoxydiols-derived secondary organic aerosol (IEPOX-SOA) from aerosol mass spectrometer measurements, Atmos. Chem. Phys., 15, 11807-11833, http://doi.org/10.5194/acp-15-11807-2015, 2015.

Hu, W. W., Hu, M., Hu, W., Jimenez, J. L., Yuan, B., Chen, W. T., Wang, M., Wu, Y. S., Chen,

C., Wang, Z. B., Peng, J. F., Zeng, L. M., and Shao, M.: Chemical composition, sources, and aging process of submicron aerosols in Beijing: Contrast between summer and winter, J. Geophys. Res., 121, 1955-1977, http://doi.org/10.1002/2015jd024020, 2016.

Huang, D. D., Li, Y. J., Lee, B. P., and Chan, C. K.: Analysis of Organic Sulfur Compounds in Atmospheric Aerosols at the HKUST Supersite in Hong Kong using HR-ToF-AMS, Environ. Sci. Technol., 49, 3672-3679, http://doi.org/10.1021/es5056269, 2015.

Jimenez, J. L., Canagaratna, M. R., Donahue, N. M., Prevot, A. S. H., Zhang, Q., Kroll, J. H., DeCarlo, P. F., Allan, J. D., Coe, H., Ng, N. L., Aiken, A. C., Docherty, K. S., Ulbrich, I. M., Grieshop, A. P., Robinson, A. L., Duplissy, J., Smith, J. D., Wilson, K. R., Lanz, V. A., Hueglin, C., Sun, Y. L., Tian, J., Laaksonen, A., Raatikainen, T., Rautiainen, J., Vaattovaara, P., Ehn, M., Kulmala, M., Tomlinson, J. M., Collins, D. R., Cubison, M. J., Dunlea, E. J., Huffman, J. A., Onasch, T. B., Alfarra, M. R., Williams, P. I., Bower, K., Kondo, Y., Schneider, J., Drewnick, F., Borrmann, S., Weimer, S., Demerjian, K., Salcedo, D., Cottrell, L., Griffin, R., Takami, A., Miyoshi, T., Hatakeyama, S., Shimono, A., Sun, J. Y., Zhang, Y. M., Dzepina, K., Kimmel, J. R., Sueper, D., Jayne, J. T., Herndon, S. C., Trimborn, A. M., Williams, L. R., Wood, E. C., Middlebrook, A. M., Kolb, C. E., Baltensperger, U., and Worsnop, D. R.: Evolution of Organic Aerosols in the Atmosphere, Science, 326, 1525-1529, http://doi.org/10.1126/science.1180353, 2009.

Kim, H., Zhang, Q., Bae, G. N., Kim, J. Y., and Lee, S. B.: Sources and atmospheric processing of winter aerosols in Seoul, Korea: insights from real-time measurements using a high-resolution aerosol mass spectrometer, Atmos. Chem. Phys., 17, 2009-2033, http://doi.org/10.5194/acp-17-2009-2017, 2017.

Kota, S. H., Park, C., Hale, M. C., Werner, N. D., Schade, G. W., and Ying, Q.: Estimation of VOC emission factors from flux measurements using a receptor model and footprint analysis, Atmos Environ, 82, 24-35, 10.1016/j.atmosenv.2013.09.052, 2014.

Kuwata, M., Zorn, S. R., and Martin, S. T.: Using Elemental Ratios to Predict the Density of Organic Material Composed of Carbon, Hydrogen, and Oxygen, Environ. Sci. Technol., 46, 787-794, http://doi.org/10.1021/es202525q, 2012.

Leong, Y. J., Sanchez, N. P., Wallace, H. W., Cevik, B. K., Hernandez, C. S., Han, Y., Flynn, J. H., Massoli, P., Floerchinger, C., Fortner, E. C., Herndon, S., Bean, J. K., Hildebrandt Ruiz, L., Jeon, W., Choi, Y., Lefer, B., and Griffin, R. J.: Overview of surface measurements and spatial characterization of submicrometer particulate matter during the DISCOVER-AQ 2013 campaign in Houston, TX, J. Air Waste Manage., 67, 854-872,

http://doi.org/10.1080/10962247.2017.1296502, 2017.

Leuchner, M., and Rappengluck, B.: VOC source-receptor relationships in Houston during TexAQS-II, Atmos Environ, 44, 4056-4067, 10.1016/j.atmosenv.2009.02.029, 2010.

Li, J. Y., Cleveland, M., Ziemba, L. D., Griffin, R. J., Barsanti, K. C., Pankow, J. F., and Ying, Q.: Modeling regional secondary organic aerosol using the Master Chemical Mechanism, Atmos. Environ., 102, 52-61, http://doi.org/10.1016/j.atmosenv.2014.11.054, 2015.

Lim, Y. B., Tan, Y., Perri, M. J., Seitzinger, S. P., and Turpin, B. J.: Aqueous chemistry and its role in secondary organic aerosol (SOA) formation, Atmos. Chem. Phys., 10, 10521-10539, http://doi.org/10.5194/acp-10-10521-2010, 2010.

Liu, J. B., Rhland, K. M., Chen, J. H., Xu, Y. Y., Chen, S. Q., Chen, Q. M., Huang, W., Xu, Q. H., Chen, F. H., and Smol, J. P.: Aerosol-weakened summer monsoons decrease lake fertilization on the Chinese Loess Plateau, Nat. Clim. Change, 7, 190-194, http://10.1038/Nclimate3220, 2017.

Mao, J. Q., Ren, X. R., Chen, S. A., Brune, W. H., Chen, Z., Martinez, M., Harder, H., Lefer, B., Rappengluck, B., Flynn, J., and Leuchner, M.: Atmospheric oxidation capacity in the summer of Houston 2006: Comparison with summer measurements in other metropolitan studies, Atmos. Environ., 44, 4107-4115, http://doi.org/10.1016/j.atmosenv.2009.01.013, 2010.

McKeen, S., Grell, G., Peckham, S., Wilczak, J., Djalalova, I., Hsie, E. Y., Frost, G., Peischl, J., Schwarz, J., Spackman, R., Holloway, J., de Gouw, J., Warneke, C., Gong, W., Bouchet, V., Gaudreault, S., Racine, J., McHenry, J., McQueen, J., Lee, P., Tang, Y., Carmichael, G. R., and Mathur, R.: An evaluation of real-time air quality forecasts and their urban emissions over eastern Texas during the summer of 2006 Second Texas Air Quality Study field study, J. Geophys. Res., 114, D00f11, http://doi.org/10.1029/2008JD011697, 2009.

Middlebrook, A. M., Bahreini, R., Jimenez, J. L., and Canagaratna, M. R.: Evaluation of Composition-Dependent Collection Efficiencies for the Aerodyne Aerosol Mass Spectrometer using Field Data, Aerosol Sci. Tech., 46, 258-271, http://doi.org/10.1080/02786826.2011.620041, 2012.

Olaguer, E. P., Kolb, C. E., Lefer, B., Rappenglueck, B., Zhang, R. Y., and Pinto, J. P.: Overview of the SHARP campaign: Motivation, design, and major outcomes, J. Geophys. Res., 119, 2597-2610, http://doi.org/10.1002/2013jd019730, 2014.

Paatero, P., Hopke, P. K., Song, X. H., and Ramadan, Z.: Understanding and controlling rotations in factor analytic models, Chemometr. Intell. Lab, 60, 253-264,

867 http://doi.org/10.1016/S0169-7439(01)00200-3, 2002.
868 Paatero, P., and Tapper, U.: Positive matrix factorization: A non-negative factor model with
869 optimal utilization of error estimates of data values, Environmetrics, 5, 111-126,
870 https://doi.org/10.1002/env.3170050203, 1994.
871 Parrish, D. D., Allen, D. T., Bates, T. S., Estes, M., Fehsenfeld, F. C., Feingold, G., Ferrare,
872 R., Hardesty, R. M., Meagher, J. F., Nielsen-Gammon, J. W., Pierce, R. B., Ryerson, T. B.,
873 Seinfeld, J. H., and Williams, E. J.: Overview of the Second Texas Air Quality Study
874 (TexAQS II) and the Gulf of Mexico Atmospheric Composition and Climate Study
875 (GoMACCS), J. Geophys. Res., 114, D00f13, http://doi.org/10.1029/2009jd011842, 2009.
876 Petters, M. D., and Kreidenweis, S. M.: A single parameter representation of hygroscopic
877 growth and cloud condensation nucleus activity, Atmos. Chem. Phys., 7, 1961-1971, ,
878 http://doi.org/10.5194/acp-7-1961-2007, 2007.
879 Petters, M. D., Wex, H., Carrico, C. M., Hallbauer, E., Massling, A., McMeeking, G. R.,
880 Poulain, L., Wu, Z., Kreidenweis, S. M., and Stratmann, F.: Towards closing the gap
881 between hygroscopic growth and activation for secondary organic aerosol - Part 2:
882 Theoretical approaches, Atmos. Chem. Phys., 9, 3999-4009,
883 http://doi.org/10.5194/acp-9-3999-2009, 2009.
884 Prenni, A. J., Petters, M. D., Kreidenweis, S. M., DeMott, P. J., and Ziemann, P. J.: Cloud
885 droplet activation of secondary organic aerosol, J. Geophys. Res., 112, D10223,
886 http://doi.org/10.1029/2006jd007963, 2007.
887 Racherla, P. N., and Adams, P. J.: Sensitivity of global tropospheric ozone and fine particulate
888 matter concentrations to climate change, J. Geophys. Res., 111,
889 https://doi.org/10.1029/2005JD006939, 2006.
890 Rollins, A. W., Smith, J. D., Wilson, K. R., and Cohen, R. C.: Real Time In Situ Detection of
891 Organic Nitrates in Atmospheric Aerosols, Environ. Sci. Technol., 44, 5540-5545,
892 http://doi.org/10.1021/es100926x, 2010.
893 Rollins, A. W., Browne, E. C., Min, K. E., Pusede, S. E., Wooldridge, P. J., Gentner, D. R.,
894 Goldstein, A. H., Liu, S., Day, D. A., Russell, L. M., and Cohen, R. C.: Evidence for NOx
895 Control over Nighttime SOA Formation, Science, 337, 1210-1212,
896 http://doi.org/10.1126/science.1221520, 2012.
897 Russell, L. M., Takahama, S., Liu, S., Hawkins, L. N., Covert, D. S., Quinn, P. K., and Bates, T.
898 S.: Oxygenated fraction and mass of organic aerosol from direct emission and atmospheric
899 processing measured on the R/V Ronald Brown during TEXAQS/GoMACCS 2006, J.

Geophys. Res., 114, D00F05, http://doi.org/10.1029/2008JD011275, 2009.

Schulze, B. C., Wallace, H. W., Bui, A. T., Flynn, J. H., Erickson, M. H., Alvarez, S., Dai, Q., Usenko, S., Sheesley, R. J., and Griffin, R. J.: The impacts of regional shipping emissions on the chemical characteristics of coastal submicron aerosols near Houston, TX, Atmos. Chem. Phys., 18, 14217-14241, http://doi.org/10.5194/acp-18-14217-2018, 2018.

Setyan, A., Zhang, Q., Merkel, M., Knighton, W. B., Sun, Y., Song, C., Shilling, J. E., Onasch, T. B., Herndon, S. C., Worsnop, D. R., Fast, J. D., Zaveri, R. A., Berg, L. K., Wiedensohler, A., Flowers, B. A., Dubey, M. K., and Subramanian, R.: Characterization of submicron particles influenced by mixed biogenic and anthropogenic emissions using high-resolution aerosol mass spectrometry: results from CARES, Atmos. Chem. Phys., 12, 8131-8156, http://doi.org/10.5194/acp-12-8131-2012, 2012.

Sullivan, A. P., Hodas, N., Turpin, B. J., Skog, K., Keutsch, F. N., Gilardoni, S., Paglione, M., Rinaldi, M., Decesari, S., Facchini, M. C., Poulain, L., Herrmann, H., Wiedensohler, A., Nemitz, E., Twigg, M. M., and Collett Jr, J. L.: Evidence for ambient dark aqueous SOA formation in the Po Valley, Italy, Atmos. Chem. Phys., 16, 8095-8108, http://doi.org/10.5194/acp-16-8095-2016, 2016.

Sun, Y. L., Zhang, Q., Schwab, J. J., Demerjian, K. L., Chen, W. N., Bae, M. S., Hung, H. M., Hogrefe, O., Frank, B., Rattigan, O. V., and Lin, Y. C.: Characterization of the sources and processes of organic and inorganic aerosols in New York city with a high-resolution time-of-flight aerosol mass spectrometer, Atmos. Chem. Phys., 11, 1581-1602, https://doi.org/10.5194/acp-11-1581-2011, 2011.

Sun, Y. L., Du, W., Fu, P. Q., Wang, Q. Q., Li, J., Ge, X. L., Zhang, Q., Zhu, C. M., Ren, L. J., Xu, W. Q., Zhao, J., Han, T. T., Worsnop, D. R., and Wang, Z. F.: Primary and secondary aerosols in Beijing in winter: sources, variations and processes, Atmos. Chem. Phys., 16, 8309-8329, http://doi.org/10.5194/acp-16-8309-2016, 2016.

Surratt, J. D., Gomez-Gonzalez, Y., Chan, A. W. H., Vermeylen, R., Shahgholi, M., Kleindienst, T. E., Edney, E. O., Offenberg, J. H., Lewandowski, M., Jaoui, M., Maenhaut, W., Claeys, M., Flagan, R. C., and Seinfeld, J. H.: Organosulfate formation in biogenic secondary organic aerosol, J. Phys. Chem. A, 112, 8345-8378, http://doi.org/10.1021/jp802310p, 2008.

Tai, A. P. K., Mickley, L. J., and Jacob, D. J.: Correlations between fine particulate matter (PM2.5) and meteorological variables in the United States: Implications for the sensitivity of PM2.5 to climate change, Atmos. Environ., 44, 3976-3984,

933 http://10.1016/j.atmosenv.2010.06.060, 2010.
934 Ulbrich, I. M., Canagaratna, M. R., Zhang, Q., Worsnop, D. R., and Jimenez, J. L.:
935 Interpretation of organic components from Positive Matrix Factorization of aerosol mass
936 spectrometric data, Atmos. Chem. Phys., 9, 2891-2918,
937 https://doi.org/10.5194/acp-9-2891-2009, 2009.
938 Wallace, H. W., Sanchez, N. P., Flynn, J. H., Erickson, M. H., Lefer, B. L., and Griffin, R. J.:
939 Source apportionment of particulate matter and trace gases near a major refinery near the
940 Houston Ship Channel, Atmos. Environ., 173, 16-29,
941 https://doi.org/10.1016/j.atmosenv.2017.10.049, 2018.
942 Watson, J. G.: Visibility: Science and regulation, J. Air Waste Manage., 52, 628-713,
943 http://doi10.1080/10473289.2002.10470813, 2002.
944 Wood, E. C., Canagaratna, M. R., Herndon, S. C., Onasch, T. B., Kolb, C. E., Worsnop, D. R.,
945 Kroll, J. H., Knighton, W. B., Seila, R., Zavala, M., Molina, L. T., DeCarlo, P. F., Jimenez,
946 J. L., Weinheimer, A. J., Knapp, D. J., Jobson, B. T., Stutz, J., Kuster, W. C., and Williams,
947 E. J.: Investigation of the correlation between odd oxygen and secondary organic aerosol in
948 Mexico City and Houston, Atmos. Chem. Phys., 10, 8947-8968,
949 http://doi.org/10.5194/acp-10-8947-2010, 2010.
950 Xu, L., Suresh, S., Guo, H., Weber, R. J., and Ng, N. L.: Aerosol characterization over the
951 southeastern United States using high-resolution aerosol mass spectrometry: spatial and
952 seasonal variation of aerosol composition and sources with a focus on organic nitrates,
953 Atmos. Chem. Phys., 15, 7307-7336, http://doi.org/10.5194/acp-15-7307-2015, 2015.
954 Xu, W. Q., Han, T. T., Du, W., Wang, Q. Q., Chen, C., Zhao, J., Zhang, Y. J., Li, J., Fu, P. Q.,
955 Wang, Z. F., Worsnop, D. R., and Sun, Y. L.: Effects of Aqueous-Phase and Photochemical
956 Processing on Secondary Organic Aerosol Formation and Evolution in Beijing, China,
957 Environ. Sci. Technol., 51, 762-770, http://doi.org/10.1021/acs.est.6b04498, 2017.
958 Ying, Q., Li, J. Y., and Kota, S. H.: Significant Contributions of Isoprene to Summertime
959 Secondary Organic Aerosol in Eastern United States, Environ. Sci. Technol., 49,
960 7834-7842, http://doi.org/10.1021/acs.est.5b02514, 2015.
961 Zhang, Q., Jimenez, J. L., Canagaratna, M. R., Ulbrich, I. M., Ng, N. L., Worsnop, D. R., and
962 Sun, Y. L.: Understanding atmospheric organic aerosols via factor analysis of aerosol mass
963 spectrometry: a review, Anal. Bioanal. Chem., 401, 3045-3067,
964 https://doi.org/10.1007/s00216-011-5355-y, 2011.
965 Zhang, Q. J., Beekmann, M., Freney, E., Sellegri, K., Pichon, J. M., Schwarzenboeck, A.,

966 Colomb, A., Bourrianne, T., Michoud, V., and Borbon, A.: Formation of secondary organic
967 aerosol in the Paris pollution plume and its impact on surrounding regions, Atmos. Chem.
968 Phys., 15, 13973-13992, http://doi.org/10.5194/acp-15-13973-2015, 2015.
969 Zhu, Q., He, L. Y., Huang, X. F., Cao, L. M., Gong, Z. H., Wang, C., Zhuang, X., and Hu, M.:
970 Atmospheric aerosol compositions and sources at two national background sites in
971 northern and southern China, Atmos. Chem. Phys., 16, 10283-10297,
972 http://doi.org/10.5194/acp-16-10283-2016, 2016.
973 Zorn, S. R., Drewnick, F., Schott, M., Hoffmann, T., and Borrmann, S.: Characterization of the
974 South Atlantic marine boundary layer aerosol using an aerodyne aerosol mass spectrometer,
975 Atmos. Chem. Phys., 8, 4711-4728, http://doi.org/10.5194/acp-8-4711-2008, 2008.
976
977
978

Table 1 Statistics of meteorological parameters, gas-phase pollutants, NR-PM_1 species, and PMF OA factors for the winter and summer campaigns at UHSL.

Variables		Season	Ave. value ± 1 SD	Minimum value	Maximum value
Meteorological parameters	Temp (˚C)	Winter	9.3 ± 6.0	0.7	25.9
		Summer	23.6 ± 3.8	12.2	33.1
	RH (%)	Winter	76 ± 18	23	99
		Summer	72 ± 19	21	98
	WS (m s^{-1})	Winter	2.1 ± 1.4	6.8×10^{-3}	9.4
		Summer	2.1 ± 1.2	9.0×10^{-3}	6.7
	Radiometer (W m^{-2})	Winter	0.6 ± 0.9	0.02	3.6
		Summer	1.1 ± 1.3	0.02	4.6
Gas-phase pollutants (ppb)	O_3	Winter	23.0 ± 12.6	0.12	53.0
		Summer	34.9 ± 15.3	0.02	75.9
	CO	Winter	238.7 ± 71.9	98.5	621.1
		Summer	168.3 ± 75.5	103.6	1110.2
	SO_2	Winter	1.0 ± 1.9	5.7×10^{-3}	29.5
		Summer	0.7 ± 1.7	2.8×10^{-3}	30.9
	NO	Winter	4.3 ± 6.4	2.0×10^{-3}	74.9
		Summer	1.3 ± 4.6	0.01	68.1
	NO_2	Winter	12.5 ± 9.7	0.8	101.2
		Summer	4.6 ± 6.4	0.2	44.4
	NO_y	Winter	22.9 ± 19.6	2.8	210.9
		Summer	8.6 ± 11.9	1.3	123.9
NR-PM_1 species (μg m^{-3})	OA	Winter	2.3 ± 1.4	0.42	9.4
		Summer	1.7 ± 1.4	0.27	12.3
	Sulfate	Winter	1.4 ± 0.8	0.05	3.4
		Summer	1.3 ± 0.6	0.02	5.6
	Nitrate	Winter	1.4 ± 1.4	0.02	6.9
		Summer	0.08 ± 0.1	0.01	0.9
	Ammonium	Winter	0.9 ± 0.6	BDL[a]	2.8
		Summer	0.5 ± 0.2	0.02	1.8
	Chloride	Winter	0.06 ± 0.09	BDL	1.1
		Summer	0.02 ± 0.02	BDL	0.5
OA factors (μg m^{-3})	HOA	Winter	0.3 ± 0.4	0[b]	8.6
		Summer	0.2 ± 0.5	0	10.9
	BBOA	Winter	0.6 ± 0.6	0	3.7
		Summer	0.1 ± 0.3	0	5.4
	COA	Winter	0.5 ± 0.5	0	4.8
	LO-OOA	Winter	0.4 ± 0.5	0	2.1
		Summer	0.7 ± 0.9	0	6.7
	MO-OOA	Winter	0.5 ± 0.3	0	1.8
		Summer	0.3 ± 0.2	0	1.6

[a]BDL: below detection limit; [b]Statistically determined factor concentrations with values below $1.0\text{x}10^{-3}$ are listed as 0.

984 **Table** 2 Correlation (*r*) of OOA mass spectra with previously published spectra database.
985 (http://cires1.colorado.edu/jimenez-group/HRAMSsd/)

Factor	Winter		Summer		Reference
	MO-OOA	LO-OOA	MO-OOA	LO-OOA	
aq-OOA[a]	**0.96**	0.75	**0.96**	**0.95**	Sun et al., 2016
MO-OOA	0.85	0.87	0.89	0.77	Setyan et al., 2012
MO-OOA	0.98	0.92	0.98	0.60	Hu et al., 2015
LV-OOA	0.97	0.91	0.98	0.62	Crippa et al., 2013
SV-OOA	0.65	0.70	0.70	0.78	Crippa et al., 2013
LO-OOAI, Biogenic-origin	0.83	0.84	0.86	0.76	Hu et al., 2015
LO-OOAII, Anthropogenic-origin	0.78	0.80	0.82	0.74	Hu et al., 2015

986 [a]aq-OOA is an aqueous-phase-processed SOA reported by Sun et al. (2016); LV=less volatility; SV=semi-volatile.

987

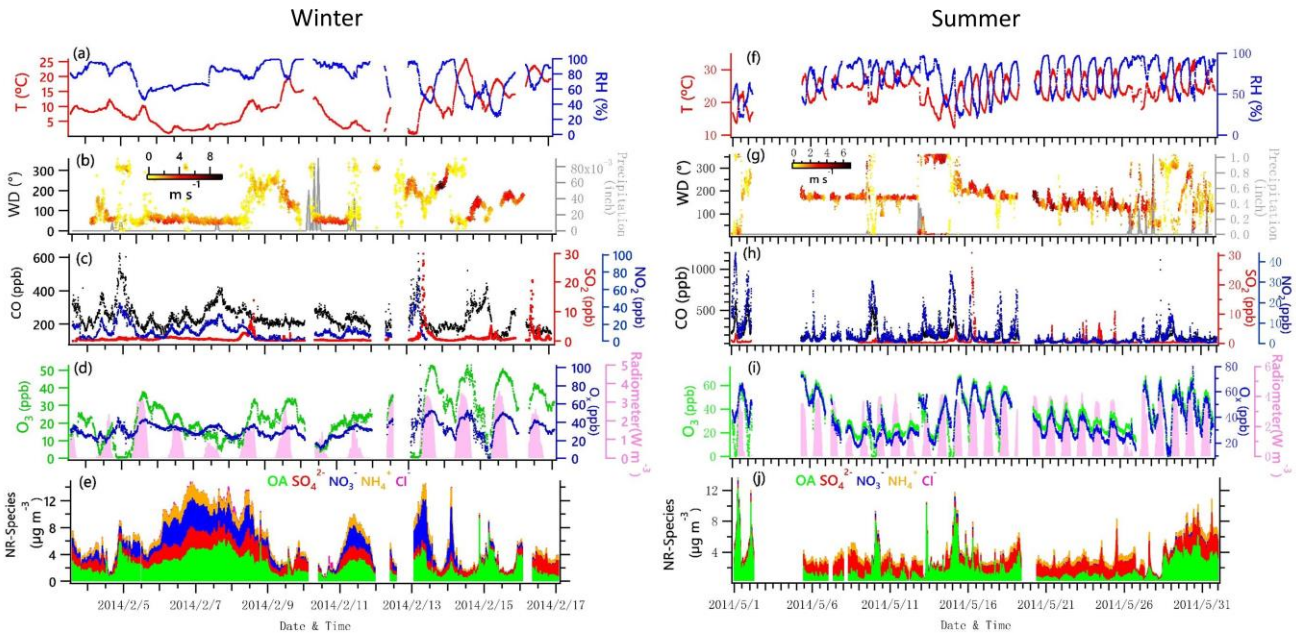

Figure 1. Time series of data collected at UHSL in Houston during the sampling periods in winter and summer 2014. Time series of 5-min average campaign data for **(a, f)** ambient temperature (T) and relative humidity (RH); **(b, g)** precipitation and wind direction (WD), with colors showing different wind speeds (WS); **(c, h)** CO, SO_2 and NO_2; **(d, i)** O_3, O_x (NO_2+O_3) and solar radiometer; **(e, j)** NR-PM_1 species, including OA, NO_3^-, SO_4^{2-}, NH_4^+, and Cl^-.

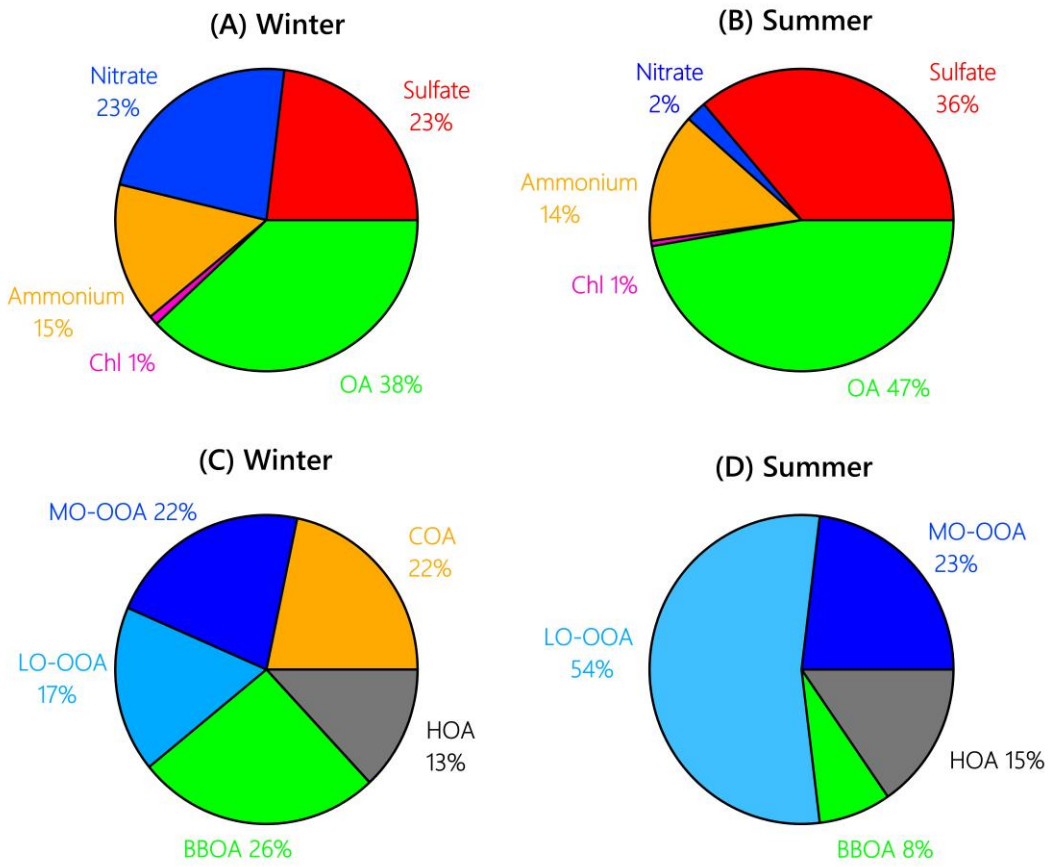

995

996 **Figure 2.** Average composition of NR-PM_1 species and OA factors during the winter (**A, C**)
997 and summer campaign (**B, D**) at UHSL.

998

999

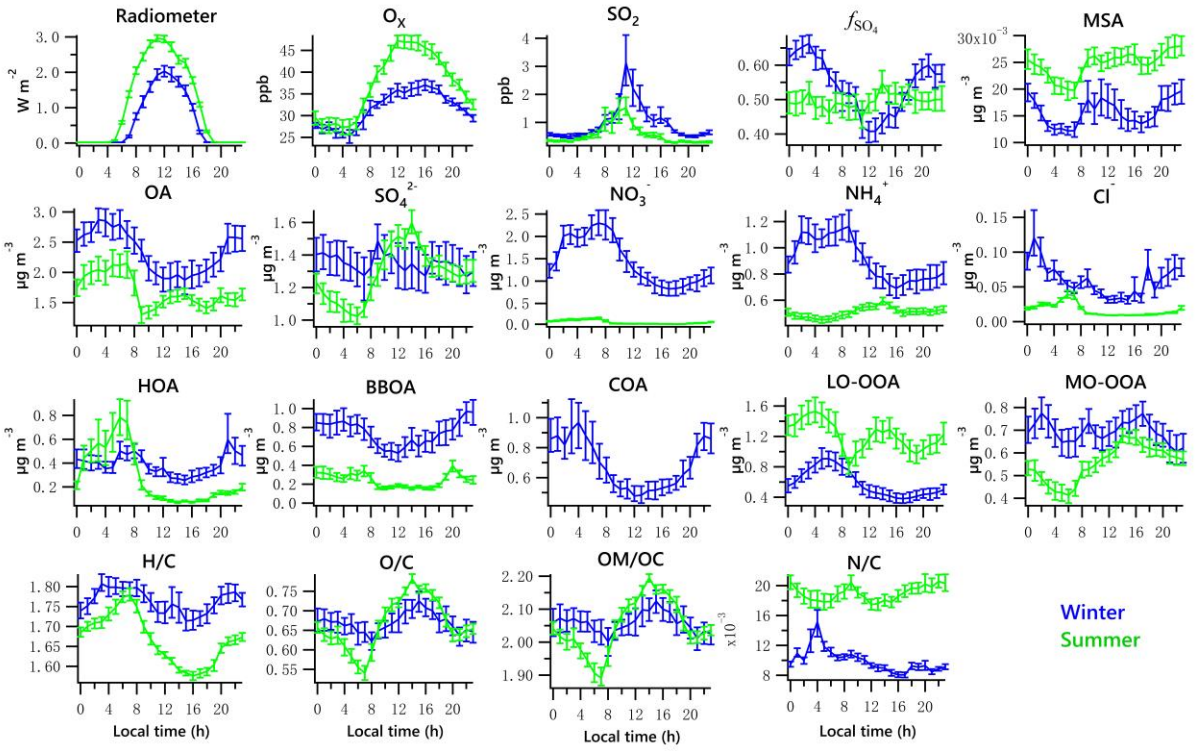

Figure 3. Diurnal profiles of radiometer, O_x, SO_2, f_{SO4}, MSA, each of the five NR-PM_1 species (Org, SO_4^{2-}, NO_3^-, NH_4^+ and Cl^-), PMF-resolved factors (HOA, BBOA, COA, LO-OOA and MO-OOA) and elemental ratios (H/C, O/C, OM/OC and N/C). Lines denote the mean value, and bars represent the 5/95 percent confidence interval in the mean (blue for winter, green for summer).

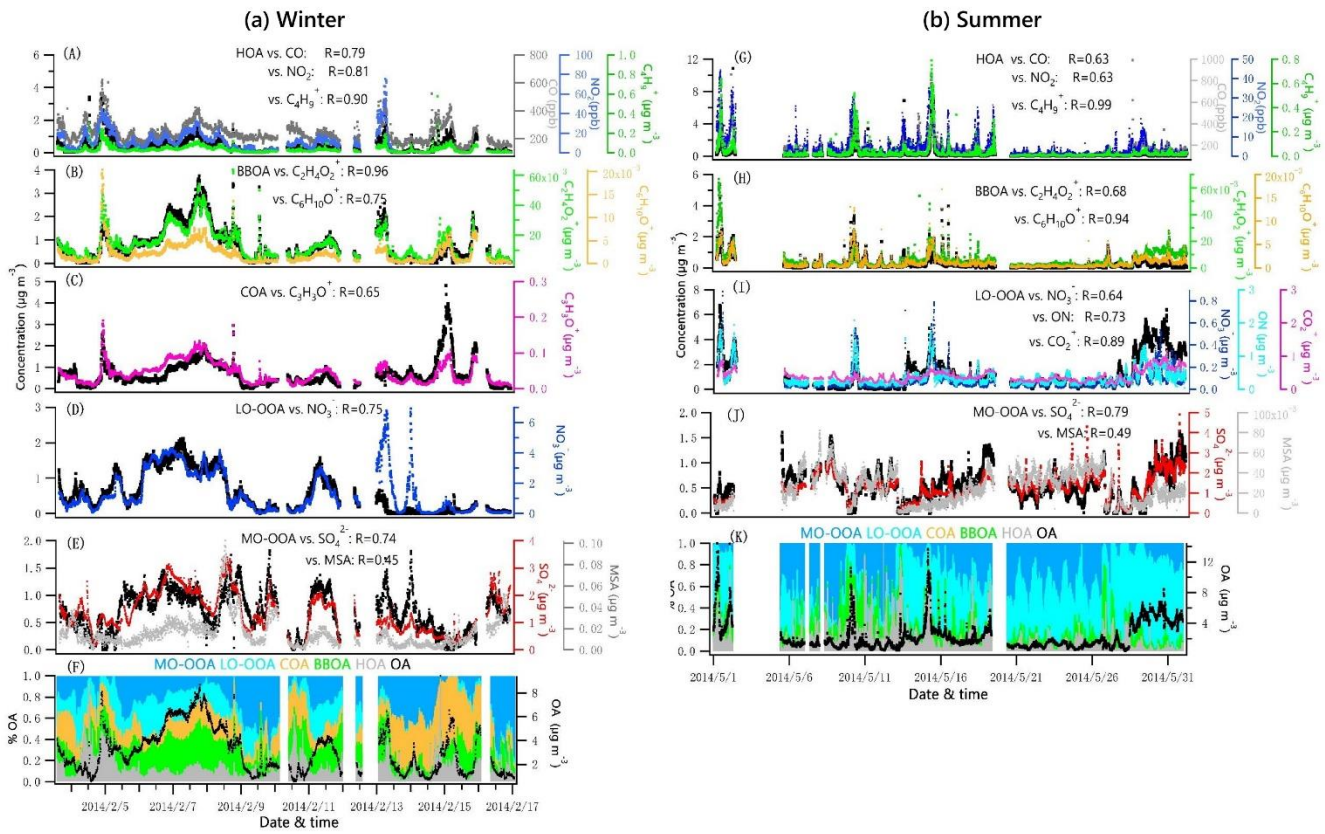

Figure 4. Time series of each OA factor and associated correlated species for the winter and summer campaign at UHSL.

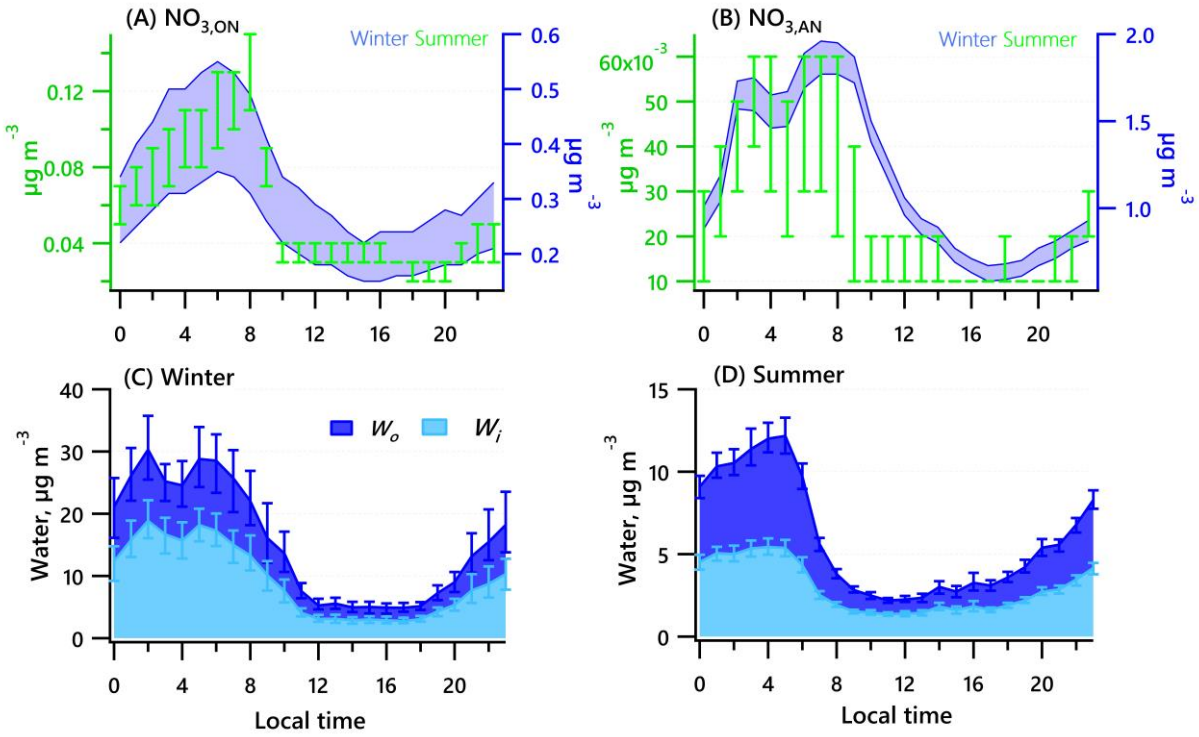

1011

1012 **Figure 5.** Diurnal profiles of the estimated range of nitrate functionality from organic nitrate (**A**)
1013 and inorganic nitrate (**B**) for the winter and summer campaigns. Estimated water associated
1014 with inorganic and organic aerosol for the winter (**C**) and summer campaigns (**D**). Solid lines
1015 denote the mean value (blue for winter, green for summer), and bars represent the 5/95 percent
1016 confidence interval in the mean.

1017

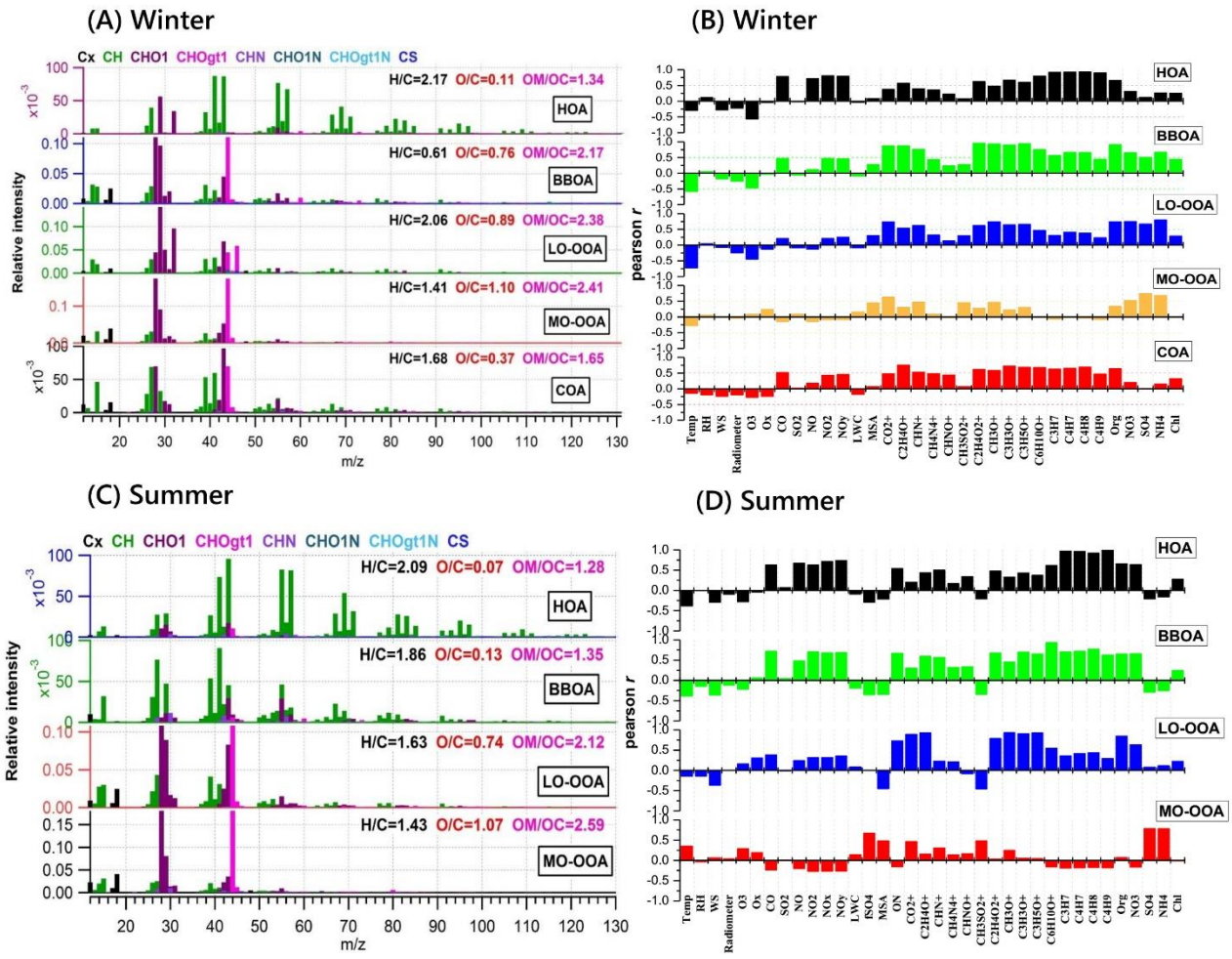

Figure 6. Mass spectra of PMF-resolved OA factors (**A**, **C**) and correlation coefficients between OA factors and other variables (tracer ions, trace gas, meteorological parameters, etc.) (**B**, **D**) for winter and summer campaigns at UHSL.

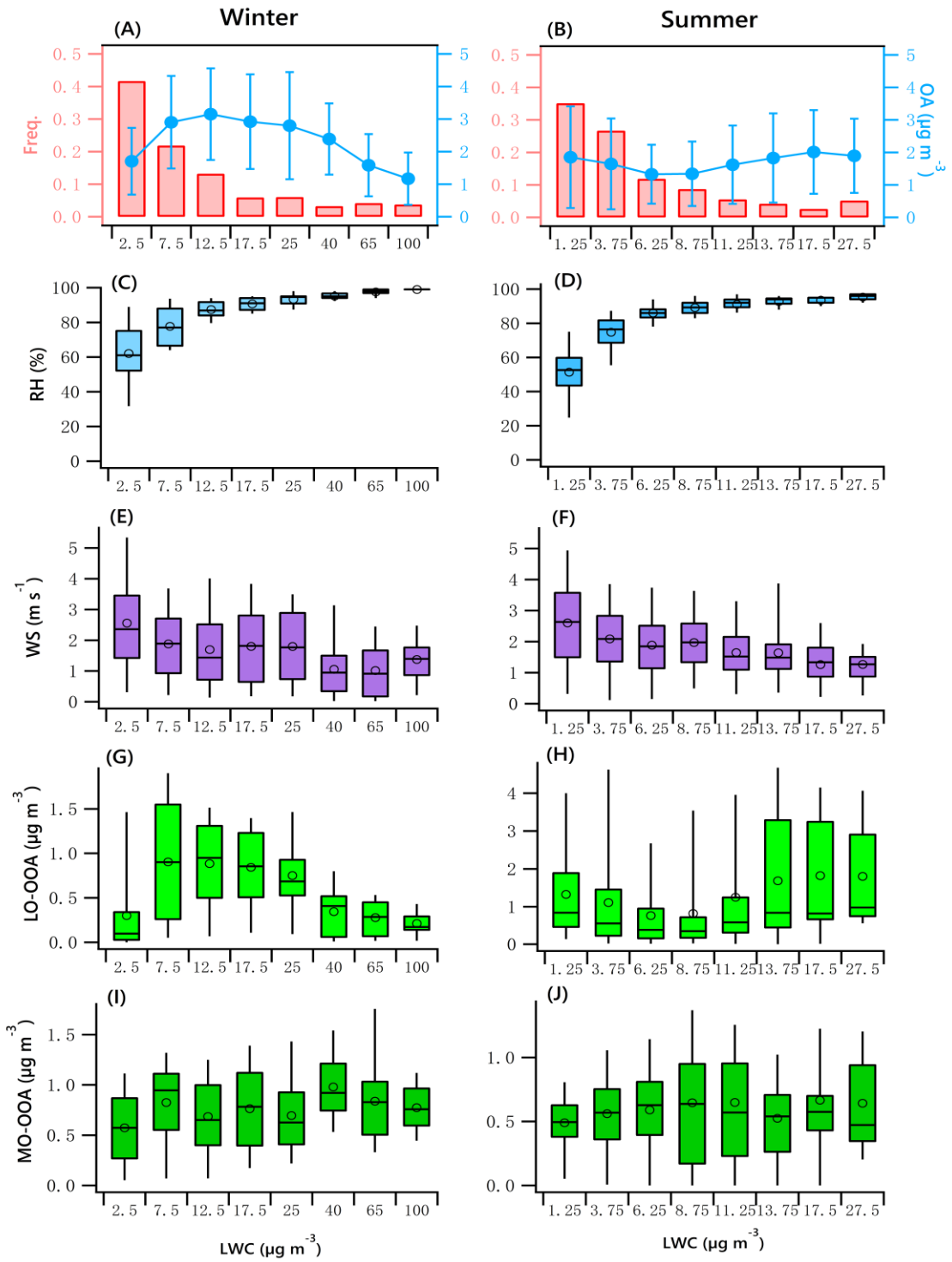

Figure 7. OA mass and frequency histograms of data points in each LWC bin for winter (**A**) and summer (**B**). Variations of RH, WS, LO-OOA and MO-OOA mass as a function of LWC in winter (**C, E, G, I**) and summer (**D, F, H, J**). The data were binned according to the LWC (with different increment values), and mean (circle), median (horizontal line), 25th and 75th percentiles (lower and upper box), and 5th and 95th percentiles (lower and upper whiskers) are displayed for data in each bin.

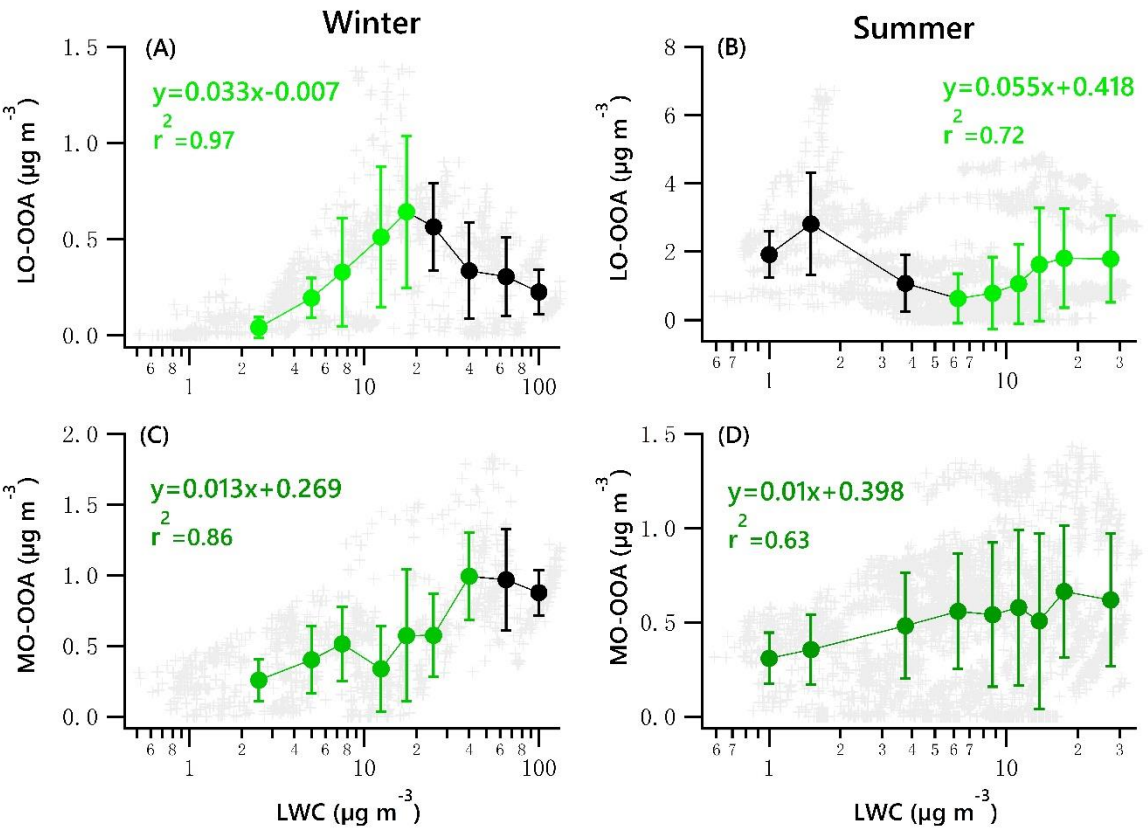

Figure 8. Scatter plots of nighttime OOA vs. LWC for the winter and summer campaign. The linear equations are given for fitting only the green dots. Solid dots denote the average value of data in each bin. Bars indicate standard deviations.

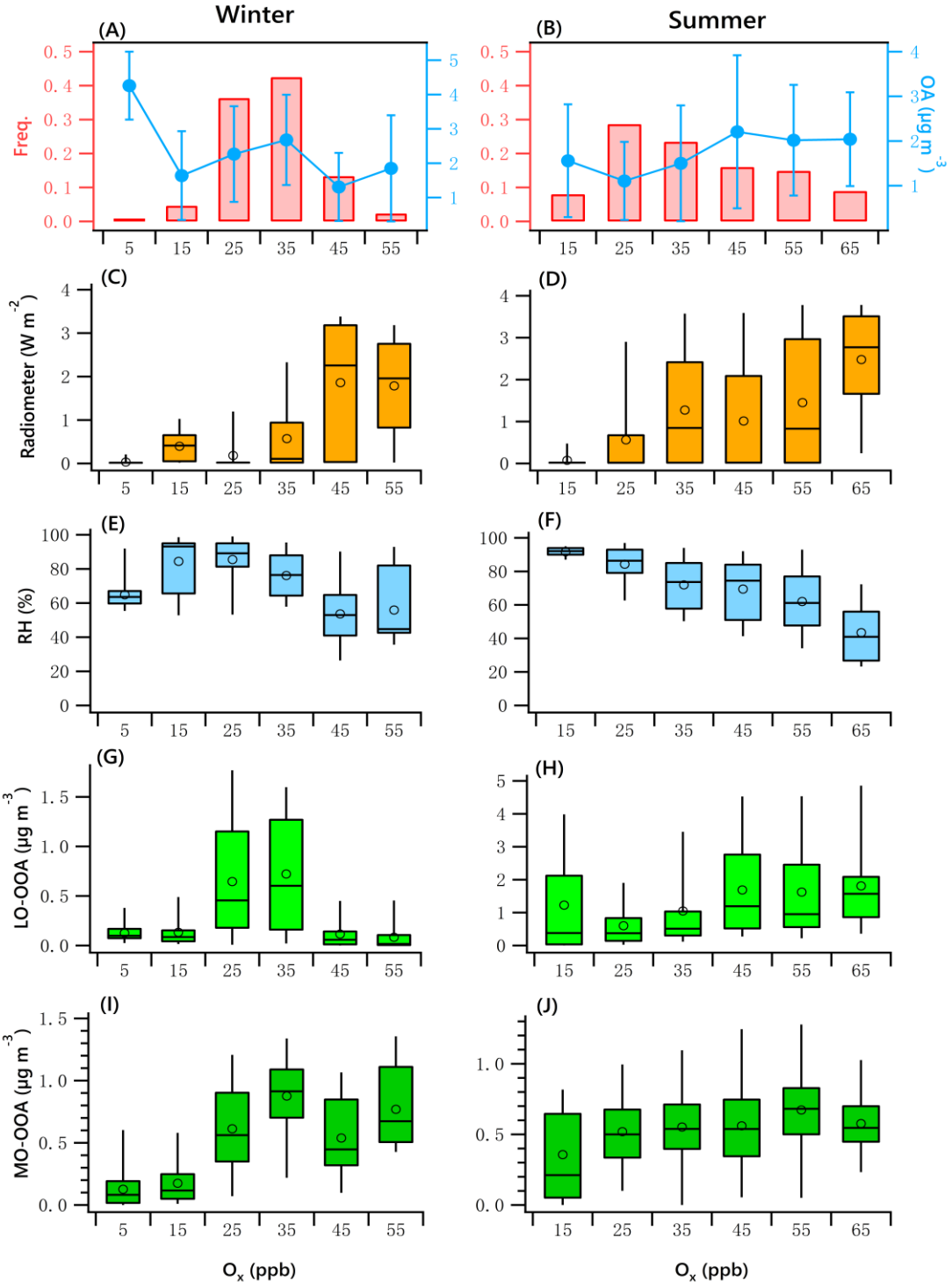

Figure 9. OA mass and frequency histograms of data points in each O_x bin for winter (**A**) and summer (**B**). Variations of solar radiation, RH, LO-OOA and MO-OOA mass as a function of LWC in winter (**C, E, G, I**) and summer (**D, F, H, J**). The data were binned according to the O_x (10 ppb increment), and mean (circle), median (horizontal line), 25th and 75th percentiles (lower and upper box), and 5th and 95th percentiles (lower and upper whiskers) are displayed for data in each bin.

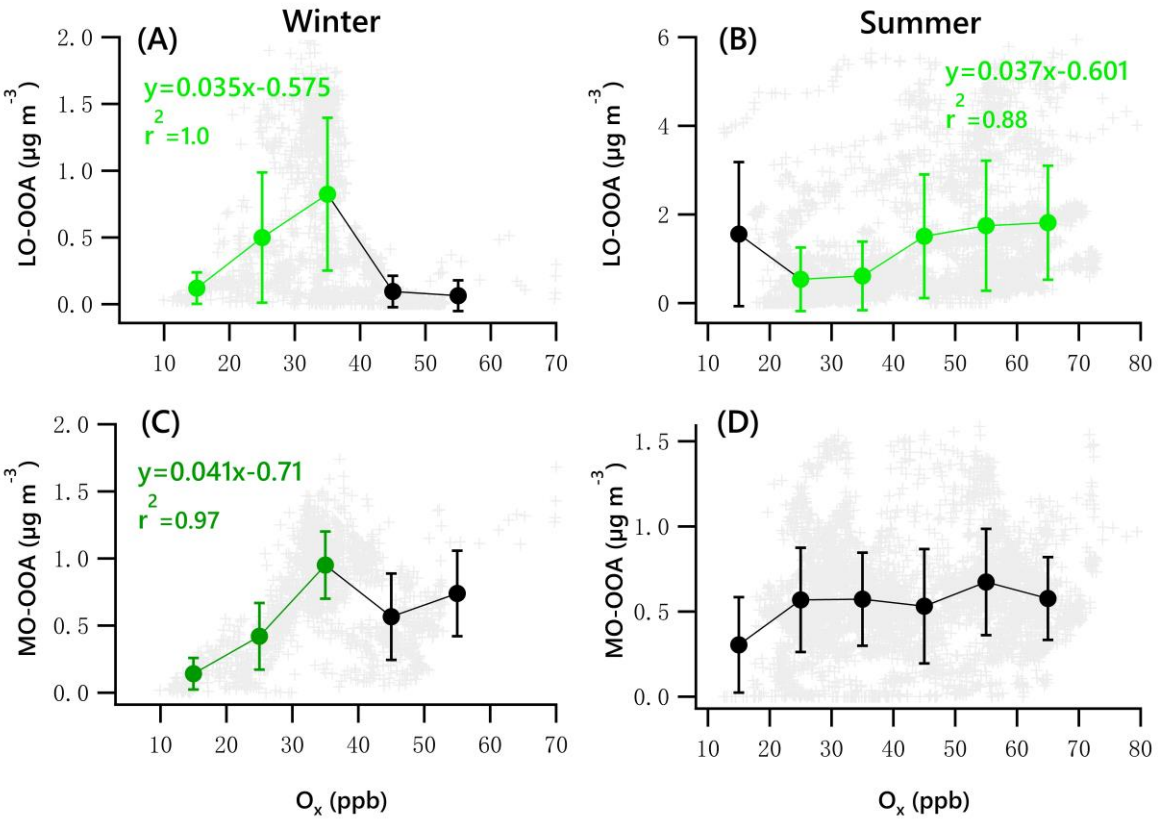

Figure 10. Scatter plots of daytime OOA vs. O_x for the winter and summer campaign. The linear equations are given for fitting the green dots. Bars indicate standard deviations.

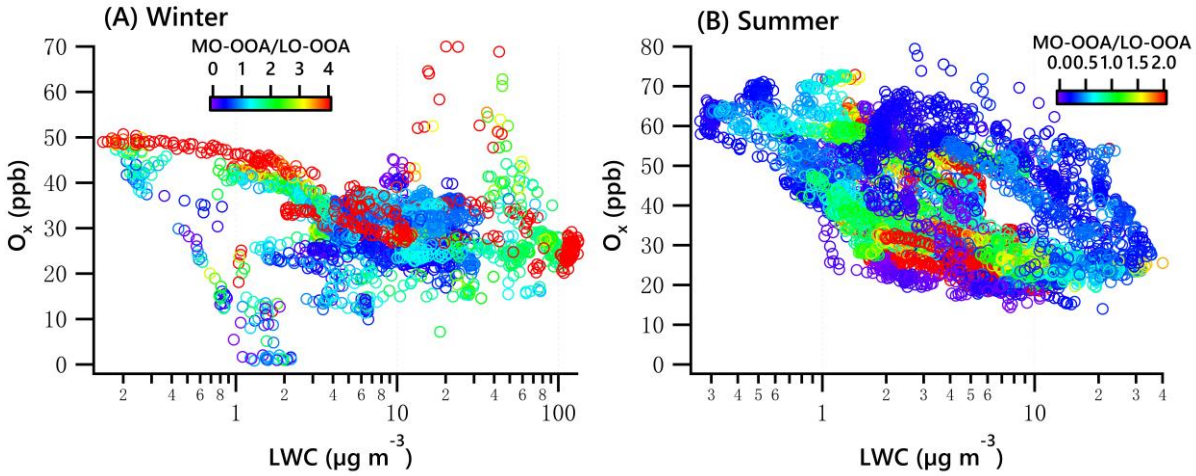

Figure 11. O_x vs LWC dependence of the ratio of MO-OOA/LO-OOA in winter (**A**) and summer (**B**).